



Methane-Derived Authigenic Carbonates on the Seafloor of the Laptev Sea Shelf

Marina D. Kravchishina^{1*}, Alla Yu Lein¹, Mikhail V. Flint¹, Boris V. Baranov¹, Alexey Yu Miroshnikov², Elena O. Dubinina², Olga M. Dara¹, Andrey G. Boev¹ and Alexander S. Savvichev³

¹ Shirshov Institute of Oceanology, Russian Academy of Sciences, Moscow, Russia, ² Institute of Geology of Ore Deposits, Petrography, Mineralogy, and Geochemistry, Russian Academy of Sciences, Moscow, Russia, ³ Federal Research Centre "Fundamentals of Biotechnology," Winogradsky Institute of Microbiology, Russian Academy of Sciences, Moscow, Russia

OPEN ACCESS

Edited by:

Tommaso Tesi,
National Research Council (CNR), Italy

Reviewed by:

Daniel Smrzka,
University of Vienna, Austria
Anna Yurchenko,
Skolkovo Institute of Science
and Technology, Russia

*Correspondence:

Marina D. Kravchishina
kravchishina@ocean.ru

Specialty section:

This article was submitted to
Marine Biogeochemistry,
a section of the journal
Frontiers in Marine Science

Received: 02 April 2021

Accepted: 25 June 2021

Published: 28 July 2021

Citation:

Kravchishina MD, Lein AY, Flint MV, Baranov BV, Miroshnikov AY, Dubinina EO, Dara OM, Boev AG and Savvichev AS (2021) Methane-Derived Authigenic Carbonates on the Seafloor of the Laptev Sea Shelf. *Front. Mar. Sci.* 8:690304. doi: 10.3389/fmars.2021.690304

Seafloor authigenic carbonate crusts are widespread in various oceanic and marine settings, excluding high-latitude basins that are corrosive to carbonate precipitation. Newly formed carbonate formations are relatively rare in modern Arctic marine sediments. Although the first-order principles of seep carbonate formation are currently quite well constrained, little is known regarding the duration or mode of carbonate formation in the Siberian Arctic shelf. Large (massive slabs or blocks) and small crusts that were micrite cemented have been recently discovered on the seafloor of the Siberian Arctic seas within the area of known seep activity in the outer Laptev Sea shelf. Cold methane seeps were detected in the area due to the presence of an acoustic anomaly in the water column (gas flares). Microbial mats, methane gas bubbles, and carbonate crusts were observed using a towed camera platform. Here, we report new geochemical and mineralogical data on authigenic shallow Siberian Arctic cold-seep carbonate crusts to elucidate its genesis. The Laptev Sea carbonate crusts mainly consist of high-Mg calcite (up to 23 mol % MgCO₃). The δ¹³C values in carbonates range significantly (from -40.1 to -25.9‰ VPDB), while the δ¹⁸O values vary in a narrow range (+4.4 ± 0.2‰ VPDB). The δ¹³C values of C_{org} that was determined from carbonates range from -40.2 to -31.1‰ VPDB. Using the isotope data and taking into account the geological setting, we consider that not only microbial but possibly thermogenic methane participated in the authigenic carbonate precipitation. Carbonate crust formation occurred below the water/sediment interface of the shallow Siberian Arctic shelf as a result of gas hydrate dissociation during Holocene warming events. The studied carbonate crusts were exhumated after precipitation into shallow subsurface shelf sediments.

Keywords: Siberian Arctic seas, biogeochemistry, methane, authigenic carbonates, carbon isotopes, cold seeps, carbonate diagenesis

INTRODUCTION

Authigenic carbonate precipitation at cold seeps is a common process (e.g., Schrag et al., 2013; Suess, 2014; Oppo et al., 2020). Due to climate change, studies regarding carbonate formation in Arctic shelf seas are of particular importance. In these seas, carbonates derived from bicarbonate, which are formed during the microbial oxidation of methane of different genesis, are relatively rare (Logvina et al., 2018; Ruban et al., 2020 and references therein). Methane is a potent greenhouse gas (Weber et al., 2019). Its increase in the atmosphere may lead to positive feedbacks with global warming (Yvon-Durocher et al., 2014; Dean et al., 2018). Anaerobic oxidation of methane (AOM), which favors in authigenic carbonate formation, is a filter that reduces the natural emission of methane acting as a carbon sinks (e.g., Devol and Ahmed, 1981; Boetius et al., 2000; Valentine, 2002; Peckmann and Thiel, 2004; Reeburgh, 2007; Knittel and Boetius, 2009). Ultimately, the contribution of the ocean to the global balance of methane in the atmosphere is very small. Estimates vary from approximately 6–3% (Weber et al., 2019) to 2% (Egger et al., 2018) or less (0.07%, Mau et al., 2017). The Arctic is characterized by a significant number of methane sources reviewed in a paper (O'Connor et al., 2010) and discussed in papers (Fisher et al., 2011; Shakhova et al., 2014; James et al., 2016; Skorokhod et al., 2016; Thornton et al., 2016; Mau et al., 2017), and elevated atmosphere background concentration of methane; its mean latitudinal value was approximately 1.85 ppm (Shakhova et al., 2010; Thornton et al., 2016). Footprints of local methane emissions were observed in the atmosphere above the Siberian shelf (Skorokhod et al., 2016; Thornton et al., 2016; Pankratova et al., 2018).

Cold methane seeps (methane-rich gas/fluid-escape from sediment) were discovered 35 years ago in the Gulf of Mexico at a depth of 3,200 m (Paull et al., 1984) and in the Oregon subduction zone located in the eastern Pacific Ocean margin at a depth of 2,036 m (Kulm et al., 1986). Subsequently, methane seeps have been discovered in all the oceans (Peckmann and Thiel, 2004; Ruff et al., 2015; Smrzka et al., 2019). To date, many studies have investigated various aspects of authigenic carbonate mineralization and overall methane seepage system functioning. These studies have been reviewed in several papers (Lein, 2004; Judd and Hovland, 2007; Roberts and Feng, 2013; Suess, 2014; Levin et al., 2016; Åström et al., 2020).

Carbonates formed due to methane (and its homologs) oxidation under anaerobic conditions (or under aerobic conditions, given the strong methane influx) occur in regions with focused hydrocarbon fluid discharge. Carbonate mineralization in the seas of the Siberian Arctic has been previously studied (Schubert et al., 1997; Galimov et al., 2006; Lein et al., 2013; Krylov et al., 2015; Kravchishina et al., 2017; Logvina et al., 2018). Different types of authigenic carbonates formed during the anaerobic oxidation of methane (AOM) of various origins were found in the Laptev Sea sediments (Kravchishina et al., 2017; Logvina et al., 2018).

Stable isotopes of C and O, petrography, and the mineralogy of methane-derived authigenic carbonates (MDAC) in the Arctic seas have been examined in several studies (Pauly, 1963;

Schubert et al., 1997; Lein et al., 1999; Kravchishina et al., 2017; Savvichev et al., 2018a, etc.). MDAC were found as Mg-calcite cement and pavement-forming crusts at the sediment–water interface of various high latitudinal seas, such as in the North Sea at depths of 120–300 m (Crémière et al., 2016b; Mazzini et al., 2016), in the Norwegian Sea at 220 m (Sauer et al., 2017), and in the Barents Sea at 220–400 m (Crémière et al., 2016a; Hong et al., 2017; Argentino et al., 2021). They were also observed in other climatic zones, such as the Green Canyon in the northern Gulf of Mexico (Bian et al., 2013). Overall, the dominant mineral phases are Mg-calcite and aragonite in cold seep carbonates (see review in Suess, 2014). MDACs with predominating aragonite cement typically form at or close to the seafloor (Suess, 2014), where sufficiently high sulfate concentrations inhibit high-Mg calcite formation (e.g., Bohrmann et al., 1998; O'Reilly et al., 2014; Prouty et al., 2016).

Recently, reports of MDAC in high-latitude seas have increased (Joseph et al., 2013; Crémière et al., 2016a; Hong et al., 2017; Kravchishina et al., 2017; Sauer et al., 2017; Åström et al., 2018). The main goals of studying the MDAC is dating the carbonates to reconstruct the history of seepage, and study the mineralogy or geochemistry to get information regarding the paleo-Sulfate-Methane Transition Zone (SMTZ) depth, and the reconstruction and modeling of their formation processes. Both spatial and temporal changes have been demonstrated in methane flow and the associated formation of the MDAC (Sauer et al., 2017).

According to Himmler et al., 2019, three carbonate-forming methane flows in the Arctic are revealed: (i) during the Penultimate Glacial Maximum, (ii) during an interstadial in the last glacial, and (iii) in the aftermath of the Last Glacial Maximum. Although the onset of MDAC formation is difficult to establish, Crémière et al., 2016a report that U-Th age (17.5 ± 0.7 ka) of seep carbonates coincide with the deglaciation of the southwestern Barents Sea (approximately 18–16 ka). The widespread methane seepage since the Last Glacial Maximum over the past approximately 20–5 ka was revealed in the European Arctic based on U-Th dating of the MDAC (Himmler et al., 2019). During this period, methane released by hydrate destabilization migrated toward the seafloor (Crémière et al., 2016a). Gas hydrate reservoirs in the European Arctic shelf were affected by the following distinct episodes: subglacial growth (during the glacial epoch) and subsequent dissociation into interglacial stages that controlled the methane release over the timescale of millennia (Serov et al., 2017). Thus Arctic deep-water gas reservoirs are sensitive to temperature variations over Quaternary time scales (Himmler et al., 2019). The MDAC should be considered as an archive of information on the long-term evolution of fluid flow in methane seeps (Bian et al., 2013). There are limited data on the precise chronology of past methane emission episodes in the Arctic from which the geological factors controlling methane release may be inferred (Himmler et al., 2019). Data on the U-Th age of the MDAC for the Siberian Arctic seas are currently unavailable.

The Laptev Sea is partly underlain by thawing remnant permafrost from the last glacial maximum (Romanovskii and Hubberten, 2006). The destabilization of intrapermafrost gas

hydrates is a possible mechanism for methane emissions in the Arctic shelf (James et al., 2016; Chuvilin et al., 2019; Puglini et al., 2020). The simulation of the permafrost-related Gas Hydrate Stability Zone (GHSZ) modeled for the Laptev Sea and East Siberian Sea shelf zones was included in Romanovskii et al. (2005, 2006). The potential thickness of GHSZ was assessed (approximately 200–250 m), and the evolution of the offshore permafrost and GHSZ under the impact of climate changes and glacioeustatic regression–transgression cycles was considered by the authors. Simulation results were compared with field observations. The results of modeling (Romanovskii et al., 2005, 2006) have shown that at present, the bases of the permafrost and GHSZ in the rifts and fault zones of the East Siberian shelf have moved to lower depths. These uplifts in areas with high oil and gas potential can serve as regions where gasses and their hydrates are concentrated and form the so-called “cryogenic traps.” The conditions for the formation of taliks have been identified in the modeling of the submarine relict permafrost. There are areas where complete dissociation of gas hydrates occurs (so-called “windows”) in the gas hydrate stability zone (GHSZ) of the East Siberian shelf. Methane discharge through the GHSZ may occur in the case when the “windows” coincide with the taliks during the transgressions (Romanovskii et al., 2006; Rekant et al., 2015; Piskunova et al., 2018). Semiletov et al. (2012) reviewed factors controlling CH₄ release from the East Siberian shelf and the hypothesis of permafrost-related Arctic hydrates.

We also acknowledge that the fate of methane in sub-seafloor Arctic Ocean reservoirs in a warming world is far from certain (James et al., 2016; Puglini et al., 2020). The faults as a system of conduits for thermogenic gas migration from deeper hydrocarbon reservoirs (Mau et al., 2017; Plaza-Faverola and Keiding, 2019) have been considered in the Laptev Sea in the recent article by Baranov et al. (2020). The presence of gas reservoirs/gas pockets is confirmed by multichannel seismic data obtained on the Laptev Sea shelf (Bogoyavlensky et al., 2018). Seepages of thermal gas from the sedimentary column into the sea water were detected at two locations at the northern margin of the shelf (Cramer and Franke, 2005).

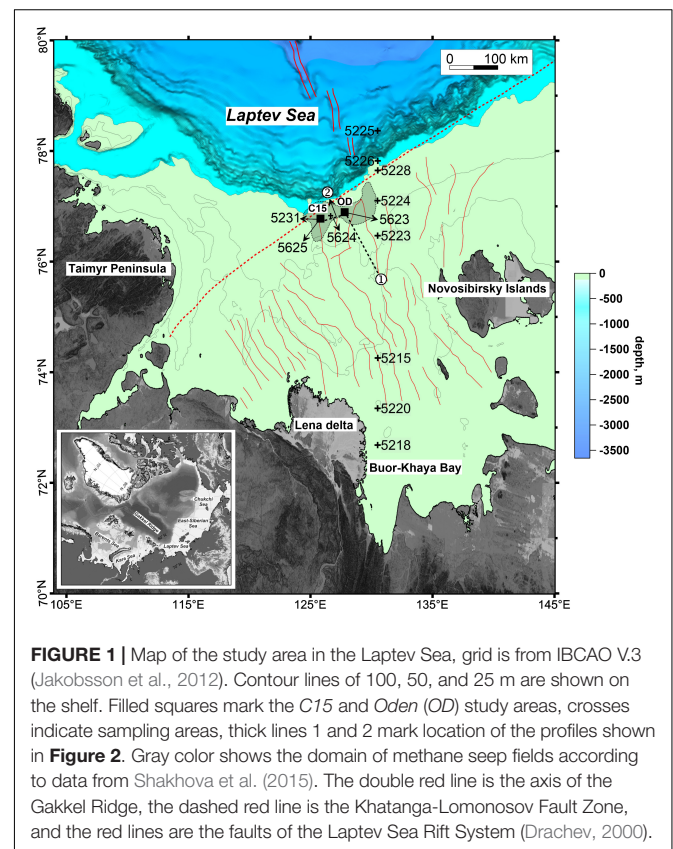
Here, we combine datasets for mineralogy and geochemistry of carbonate crusts and the surface layer of bottom sediments collected during the summer expedition of 2017 in the Laptev Sea. The objective of our research was to study the composition, morphology, and macro- and microstructure of carbonate crusts, as well as to establish the genesis of methane, which took part in the formation of authigenic carbonates.

GEOLOGICAL SETTING

Carbonate crusts have been collected by the *Sigsbee* trawl from a depth of 63 m while studying the macrofauna within the area of active methane discharge in the Laptev Sea (Vedenin et al., 2020). Carbonates have been found approximately 50 km away from the *C15* methane seep area (~50 × 50 m, 76°46.34 N and 125°49.75 E, 71 m depth), which was investigated in 2015 (Flint et al., 2016; Kravchishina et al., 2017; Demina and Galkin, 2018; Savvichev et al., 2018a).

The study area where the carbonate crusts were obtained was located on the Laptev Sea shelf. The center of the area was assigned to the location with coordinates 76.894°N and 127.798°E, where the maximum methane content in surface waters was observed (Thornton et al., 2016). These data were obtained during the summer of 2014 on the SWERUS-C3 expedition with the Swedish icebreaker *Oden*; hence, this region was called the *Oden* area (Baranov et al., 2020; Vedenin et al., 2020). Structurally, the *Oden* area is located within the Laptev Sea Rift System (Figure 1). The Laptev Sea Rift System consists of horsts and grabens, which are limited by NW-SE and N-S-striking faults, stretching from the coast to the shelf break. On the shelf break, it is intersected by the Khatanga-Lomonosov Fault Zone (KLFZ) oriented in the SW-NE direction (Drachev, 2000).

The KLFZ was identified by the geophysical field pattern and is considered a transform fault that formed in the Paleocene. It separates the oceanic lithosphere of the Eurasian Basin from the thinned continental lithosphere of the Laptev Sea (Drachev, 2000; Shipilov, 2004). The shear nature of this fault zone is established by the displacement of the horst and grabens of the Laptev Sea Rift System (Shkarubo et al., 2014). The KLFZ display evidence of modern transform fault activity (Baranov et al., 2018). North of the KLFZ, in the deep-water basin, the rifting of the Laptev Sea shelf is replaced by ultra-slow spreading on the Gakkel Ridge (Gramberg et al., 1990; Drachev, 2000; Franke et al., 2001; Gusev et al., 2002).



The relief of the Laptev Sea shelf is characterized by a system of basement depressions and heights, which have an N-S and NW-SE strike. Structurally, they correspond to rifts and horsts filled by sediments that reach up to 10–12 km (Drachev, 2000). The horsts and grabens are limited by deep-seated faults that end mainly in the Paleocene sediments. Some of these faults intersect the seafloor, forming scarps with a height of a few meters (Rekant and Gusev, 2009).

The shelf of the Laptev and East Siberian Seas are subdivided into outer and inner parts. The outer shelf was morphologically distinguished as an inclined plane along the shelf break. It is a distinct feature and, judging by the available data, is nowhere to be found except in this region of the Arctic. It is assumed that its formation was most likely due to stepwise subsidence of this continental margin under conditions of excessive sedimentary input carried by rivers flowing into the Laptev Sea (Piskarev, 2016).

In the Laptev Sea, areas of intense bubble methane discharge (cold methane seeps), which an echosounder records in the form of hydroacoustic anomalies, were first discovered during the International Siberian Shelf Study expedition between August and September 2008 (Yusupov et al., 2010). As a result of further research on the outer shelf in the northern part of the sea, 112 flare seep fields were discovered to be located in depths ranging from 50 to 90 m (Shakhova et al., 2015). These cold seeps fields form a region approximately 150 km long and up to 50 km wide (Figure 1). The *Oden* area is located within this region (Baranov et al., 2020).

MATERIALS AND METHODS

Field Observations and Sample Collection

Two large (51 × 40 cm, 5.90 kg and 40 × 30 cm, 4.99 kg) carbonate crusts (OD-I and OD-II) were collected by the *Sigsbee* trawl (2 m frame width) from a depth of 63 m during macrofauna investigations (Vedenin et al., 2020) in the Laptev Sea at station 5623, during the 69th cruise of the RV *Akademik Mstislav Keldysh* (Flint et al., 2018). The distance between the point of contact (76°53.667 N and 127°48.157 E) and the detachment of the trawl from the bottom (76°53.566 N and 127°49.075 E) was 421 m. Six relatively small (up to ~1–3 cm) fragments (OD-1–OD-6) of carbonate crusts were found during the washing of the trawl and box corer samples of the bottom sediments at the same station (5623).

The bathymetric and hydroacoustic investigations at the *Oden* seep area were performed with a Kongsberg EA600 ship-mounted single-beam echosounder operating at a constant frequency of 12 kHz. The standard software EA600 was used to control the echosounder. Hydroacoustic and bathymetric surveys were performed in the area along the separate transects, the distance between which ranged from less than 100 to 500 m.

Visual observations of the seafloor were conducted using the towed camera platform *video module* manufactured at the Shirshov Institute of Oceanology, RAS (IO RAS). The *video module* consists of several main hulls with electronic equipment,

batteries, and video cameras towed at a speed of 0.5 knots. Videos were recorded with a high-resolution BEWARD BD 3270Z camera and stored electronically in AVI format.

Full-depth water column profiling was performed at stations using an SBE 911 Plus probe. Bottom sediment sampling was performed from a depth of 55–70 m using a *van Veen* grab sampler (0.1 m² sampling area), box corer grab, *Niemistö* corer (Niemistö, 1974), and a gravity corer within the seepage area at stations 5623, 5624, 5625, 5231, 5224, and 5223 (Figure 1). The coordinates and depth of the stations are given in the corresponding tables of the section Results. Mini cores with a length of up to 15 cm were selected by plexiglass tubes from the bottom grab samples at stations 5623, 5624, and 5625 collected adjacent to the crusts. Mineralogical identification by XRD, carbon content, XRF, and stable isotope analyses were performed in these sediment samples. All the sediment samples were examined using an Olympus BX-51 polarization microscope by the smear-slide method onboard (Rothwell, 1989). The type of sediment was determined according to the Bezrukov and Lisitzin (1960) classification of sea bottom sediments (Lisitzin, 1996).

Petrography and Mineralogy

The carbonate samples were washed to remove any attached uncemented sediments and dried at 30°C prior to analysis. The examined samples are typically highly macroscopically homogeneous, and samples of this size are contaminated by clastic material. The composition, texture, structural features, and microstructure of carbonate crusts have been studied using various methods. We focused our detailed analyses on the collected large crusts (or blocks). Carbonates were examined using a Carl Zeiss Stemi 508 binocular microscope.

Carbonate petrography of thin sections was investigated using an Olympus BX-51 polarization microscope with a digital microphotographic system based on an Olympus Camedia C5050 camera with Image Scope S software.

The composition of the carbonates was studied in bulk and hand-drilled sub-samples. Sub-samples of approximately 1 cm³ in volume of macroscopically homogeneous matter (referred to as “bulk” samples hereafter) were collected from larger crust samples (OD-I-1, OD-I-2, and OD-I-3) to quantify within-crust compositional variability. Hand drilled sub-samples of the micrite matrix and mineral inclusions (sample OD-I-1) were also sampled. Sub-samples were finely crushed in an agate mortar and the same “bulk” powder was used for X-ray diffraction (XRD), X-ray fluorescence (XRF) analysis, and stable carbon and oxygen isotope determinations.

Three sediment samples were analyzed to assess the composition of the clastic end-member. They were collected using the *van Veen* grab sampler in the study area and away from the active zones of fluid seepage. These samples (stations 5623 – *Oden* area, 5624, 5625) were retrieved from depths of 45 to 70 m. The average mineral and elemental compositions were assumed to be representative of the sediment fraction incorporated within the carbonates.

Mineralogy was determined on milled and homogenized bulk powders from 24 carbonate sub-samples and 3 bottom sediment samples impacted by seepage. The specific phases

(14 in total) were microscopically detected and micro-drilled from carbonates and analyzed as well by the same way. Detailed mineralogical identification by XRD was performed on unoriented prepared specimens analyzed by a Bruker D8 Advance diffractometer (BRUKER AXS, Germany) (Cu K_{α} with Ni 0.02 filter, 40 kV, 40 mA, with a linear detector LYNXEYE with scanning in a discrete mode with a 0.02° steps, exposure 4 s/step in a range of 2.5° – 70° 2θ range) in IO RAS. Mineral identification was performed with an automatic/manual peak search using BRUKER's Diffrac EVA 3.1. The PDF4 Mineral database of ICDD and the Crystallographic Open Database (COD) were used for identification purposes. Mineral quantification was performed by Rietveld refinement using the TOPAS 5 software. The refined parameters included background coefficients, sample displacement, scale, and unit cell parameters of all phases, as well as the preferred orientation. Depending on the mineral phase, the lower limit of quantification is commonly 1–2 wt. % and the uncertainty 2–3 wt. %. The calcite Mg content (MgCO₃ mol %) was estimated from the unit cell parameter d104 value according to Bischoff et al. (1983) and Zhang et al. (2010).

Rock chips were examined using a VEGA-3 sem TESCAN (Czech Republic) scanning electron microscopy (SEM) with an energy dispersive X-ray spectrometer (EDS), Oxford INCA Energy 350 (United Kingdom).

Carbon Content and XRF

The contents of C_{org} and C_{tot} were determined by an automatic coulometric method using an AN 7560 carbon analyzer (Russia) in the same bulk powder of 18 carbonate and 9 bottom sediment samples impacted by seepage. For the C_{tot} analysis, approximately 300 mg of the bulk subsample was combusted at $1,350^{\circ}\text{C}$, and the production of CO₂ was quantified. For C_{org} determination, approximately 400 mg of the same “bulk” powder was placed in carbon-free pervious ceramic combustion boats. The samples were placed on a heating plate at 50°C , and samples treated with 10 vol.% hydrochloric acid (HCl) to remove inorganic carbon (carbonate) and subsequently rinsed with distilled water and dried in the drying oven prior to analysis in the same manner as C_{tot} . The results are given in weight percent (wt.%). The accuracy of the method was $\pm 5\%$. The calcium carbonate content was calculated as $\text{CaCO}_3 = (C_{tot} - C_{org}) \times 8.33$.

X-ray fluorescence (XRF) analysis of “bulk” powder of 24 carbonate and 5 bottom sediment samples impacted by seepage was performed on a sequential spectrometer with wavelength dispersion, model PW 2400 (Philips Analytical), and software (SuperQ, PANalytical). Detrital contents in the carbonate crusts were estimated simply by summing the contents of K₂O, Fe₂O₃, SiO₂, TiO₂, and Al₂O₃ (Bayon et al., 2009).

Stable Isotope Analyses

Stable carbon and oxygen isotope analyses of 12 “bulk” powder carbonate (samples OD-I-2 and OD-I-3) were performed at the Laboratory of Isotope Geochemistry and Geochronology in Institute of Geology of Ore Deposits, Petrography, Mineralogy, and Geochemistry, RAS (IGEM RAS, Russia). The analysis was

performed using the Delta V+ CF IRMS with the GasBenchII option (Thermo Fisher Scientific). For analysis, approximately 250 μg of powdered bulk carbonate was used. The common phosphoric acid technique was applied to liberate CO₂ from the carbonates. All samples were measured both with and without pre-treatment with 10% H₂O₂ solution (boiling for 1 h) to check the possibility of organic carbon contamination. Carbonates pre-treated with H₂O₂ were washed three times with distilled water and carefully dried at 60°C . The accuracy in determining the $\delta^{13}\text{C}$ and $\delta^{18}\text{O}$ values was ± 0.04 , and ± 0.06 , respectively.

The stable carbon isotope composition ($\delta^{13}\text{C-C}_{org}$ and $\delta^{13}\text{C-CaCO}_3$ values) of “bulk” powder of 18 carbonate (sample OD-I-1) and 9 bottom sediment samples impacted by seepage were determined in Federal Research Center “Fundamentals of Biotechnology”, RAS (FRC Biotechnology, Russia). For analysis, approximately 250 μg of the bulk carbonate was used. To analyze the stable carbon isotope ratio of CaCO₃, the samples were treated with hot HCl (1: 4) (Yu et al., 2018), and the released CO₂ was absorbed with a concentrated Ba(OH)₂. The formed BaCO₃ precipitate was used to determine the isotopic composition of the initial $\delta^{13}\text{C-CaCO}_3$ using a Delta Plus XP mass spectrometer (Thermo, Germany) with an accuracy better than $\pm 0.1\%$. Then, the remaining samples were heated under vacuum and reacted with CuO at 900°C to analyze the stable carbon isotope ratio of C_{org} (Savvichev et al., 2018a). The released CO₂ was sealed in glass ampoules and analyzed offline using a Delta Plus XP mass spectrometer (Thermo, Germany) with an accuracy better than $\pm 0.1\%$. The carbon isotope composition of methane was determined using a TRACE GC gas chromatograph (Thermo Fisher Scientific, Germany) connected to a Delta Plus mass spectrometer in FRC Biotechnology. The accuracy of the $\delta^{13}\text{C-CH}_4$ values obtained did not exceed $\pm 0.1\%$. All $\delta^{13}\text{C}$ and $\delta^{18}\text{O}$ values obtained are reported in conventional delta (δ) units relative to the international standard Vienna Pee Dee Belemnite (VPDB).

Gas Analyses and Pore Water

Gas analyses were carried out in surface bottom sediments impacted by seepage (stations 5623, 5624, 5625, 5231, and 5224) and background surface sediments on the shelf (5216, 5218, 5215, 5223, and 5228) and on the continental slope (5225 and 5226) (Figure 1).

The dissolved methane concentration in the bottom sediments (30 samples) was determined using a headspace equilibrium degassing method with subsequent measurements using a gas chromatograph with a Kristall-200-OM flame ionization detector (Russia) with an accuracy of approximately $\pm 1\%$. The method used in our work was inspired by McAuliffe (1971) and was modified to increase the sensitivity and storage of samples prior to analysis (Lapham et al., 2017). Immediately after sampling the sediment core, 2 cm³ of the sample was transferred into glass serum vials using a syringe without a needle holder. Two KOH pellets (approximately 0.1 g) were added to each vial to stop microbial activity. Filtered seawater (through filters with 0.2 μm pore size) was added to a sign marking the volume of the tube's head

space, and the tubes were hermetically closed with gas-tight stoppers made of butyl rubber with natural caoutchouc and crimped with aluminum seals. All samples were stored upside down at room temperature and analyzed within 1 month for CH₄ concentrations.

The sediment samples for pore water analyses were collected using a *Niemistö* corer within the seepage area (station 5231), adjacent shelf area (stations 5218 and 5224 with depth from 18 to 54 m, respectively), and at the continental slope (stations 5227 and 5225 with depth more than 1900 m). The pore water was squeezed out onboard by centrifugation and aliquots were analyzed for chloride (Cl⁻ by direct titration of the sample with AgNO₃ solution), sulfate (SO₄²⁻), and calcium (Ca²⁺) using spectrophotometric methods (Grasshoff et al., 2007).

RESULTS

Seafloor Topography

The *Oden* area of approximately 13 km² is located on the outer shelf of the Laptev Sea. The outer shelf begins at a depth of 50 m and is clearly distinguished by an increase in the seafloor slope and its increased roughness compared with that of the relief of the inner shelf. Roughness manifests itself in the form of bottom topography blocks of 2–3 km in size, separated by small depressions or scarps as large as 4 m high (**Supplementary Figure 1**).

Our bathymetric survey showed that the studied area could be divided into two parts based on its morphology. The northern part is located at greater depths than the southern part (68 and 62 m, respectively) (**Figure 2A**). The boundary between the northern and southern parts is a scarp with a length of more than 3 km, which extends in the W-E direction. The height of the scarp decreases from 3 to 2 m, traveling from east to west. The scarp becomes gentler in the west compared to the east. During the hydroacoustic survey, gas flares were only found in the southern part of the study area.

Gas Flares

As a result of the hydroacoustic surveys, the gas flares (hydroacoustic indications of gas bubble emissions) were recorded only in the southern *Oden* area, where they formed a cluster of closely spaced flares. The width of the gas flares may achieve a few hundred meters; this was determined at several crossings of one of the largest gas flares. This cluster is in a field of cold methane seeps. The field is shaped like a band that extends in a WSW-ENE direction for approximately 2 km and strikes under an oblique angle to the scarp that separates the northern and southern study area (**Figures 2A,B**). The width of the gas flares can be as large as a few hundred meters, as it was determined at several crossings of one of the largest gas flares. Gas flares reaching the surface were visually observed from the vessel (**Figure 2C**). The trawling at station 5623 was carried out within the cold methane seeps field, and the trawling section passed through several gas flares where carbonate crusts and crusts were found during visual observations using a towed camera (**Figures 2D,E**).

Seabed Observations With the Video Module

The length of the video transect at *Oden* was 2,640 m, with a recording duration of 1 h 42 min and 22 s. At *C15*, the length of the video-transect reached 1,230 m (with a recording duration of 1 h 17 min 19 s).

Video transects at both sites present examples of methane seep features on the Laptev Sea outer shelf. The topography was generally smooth, with 100% sediment cover along the video transects. The bottom sediments were muds with a brown (oxidized) surface layer. Only small and local disturbances of microrelief were present, such as looseness of sediments in spots up to 1 m² in size, small gouges (grooves) 5–20 cm wide, traces of slumping on the scarp, and dark spots of sediment (apparently reduced) up to 1 m².

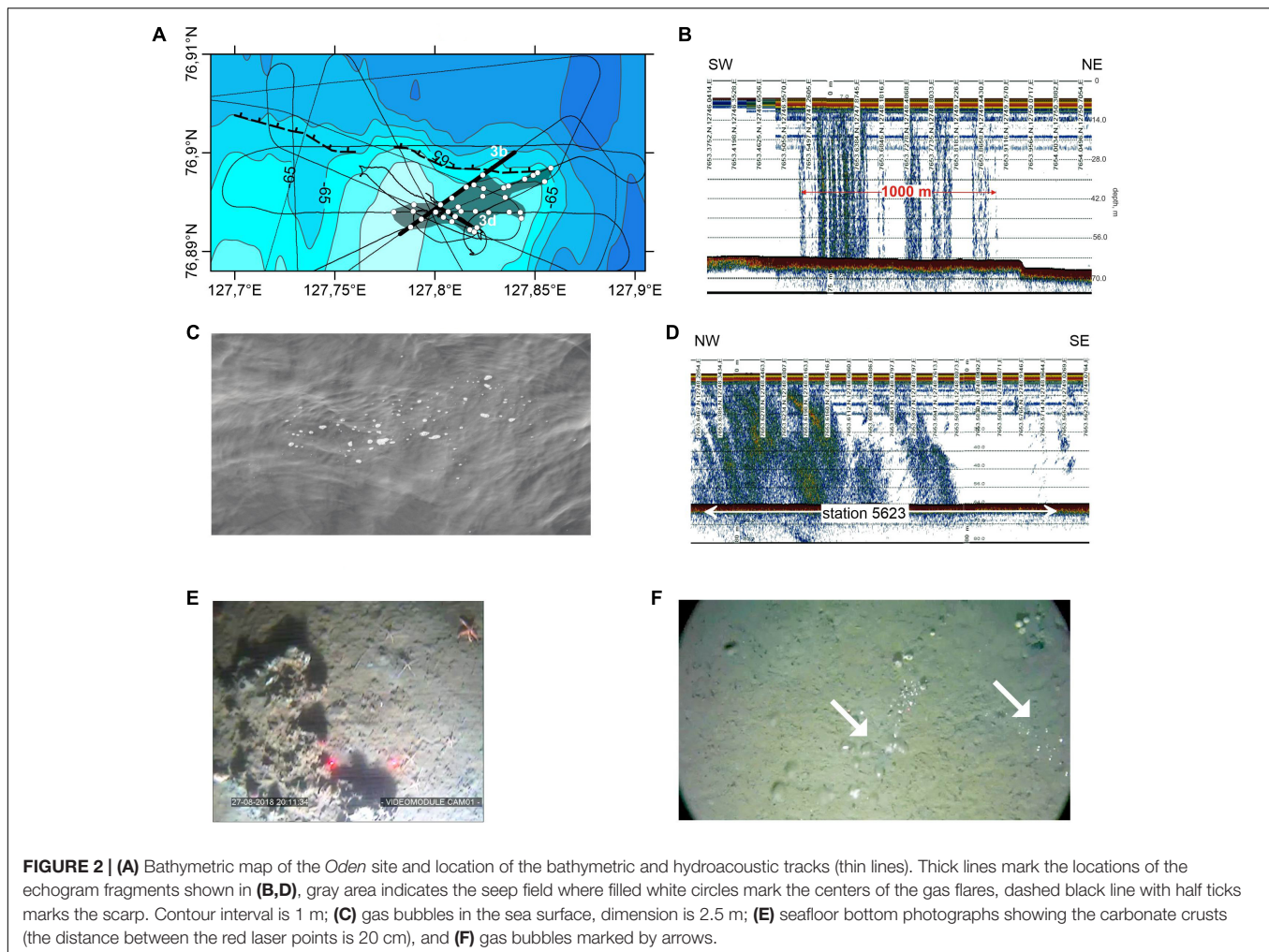
Bubble methane discharge was the most prominent evidence of seepage at the *Oden* and *C15* sites (**Figure 2F**). Methane discharge appeared as bubble chains of different intensities originating from small orifices in the sediment. Methane was emitted from a single hole, but more often, a group of three to five orifices was observed.

Carbonate crusts of different sizes and shapes provided more notable evidence of long-term methane seepage. Crust shapes varied from round to elongated or irregular. Crusts are often associated with orifices 2–3 cm in diameter or contain cracks. The crust surface color was gray, sometimes white, or dark gray. Crusts of dark gray color were slightly covered with sediment, often with numerous small rounded or angular pieces of carbonates around them or at some distance away. It may be suggested that these crusts were disintegrating and were older than crusts of white color.

Bottom Sediments Lithology and Sedimentary Environment

The upper layer (up to 20 cm) of the sediments was investigated within the study area. All box core tops consisted of soft silty-pelitic muds. The surface sediments contained approximately 10–20% fine sand-sized material. The sandy grains were poorly sorted. Terrigenous grains (quartz, feldspars, and rock fragments) were predominant. They were rounded to varying degrees, sometimes with regular faces. The clastic minerals were dominant (from 66 to 82% by XRD). Clay minerals (smectite, chlorite, and illite) and mica (muscovite) were common throughout the sediments and did not exceed 29%. Carbonate minerals are rare and present as dolomite, calcite, and Mg-calcite. Biogenic components (algae cells, detritus, calcareous, and agglutinated benthic foraminifera, sponge spicules, etc.) were found sporadically based on smear slides observations. The sediments were bioturbated with numerous Siboglinidae tube worms and burrows (e.g., fossil placements of tubeworms).

The uppermost brown (oxidized) lithological unit was approximately 0.5–2 cm. The underlying dark gray (stations 5623 and 5624) to black (st. 5625) muds were reducing. Free hydrogen sulfide gas was identified in black muds by a typical odor. A significant quantity of amorphous particles differing in high X-ray intensity for S and Fe was detected at st. 5625.



Sulfide phases (pyrite and hydrotroillite) were observed in the reduced muds. Hydrotroillite in contact with air is subjected to rapid oxidation. When exposed to the atmosphere for a sufficient time (12–48 h), the black hydrotroillite inserts a brownish color, and the dark gray sediment changed to a brownish color. Authigenic pyrite shows different morphologies: framboids (up to 20 μm) and individual grains of a rounded shape or close to the pentagonal dodecahedron form (approximately 5 μm). Fine gravel (rounded and not rounded) was occasionally found in the reduced muds. The transition layer between two lithological units (oxidized and reduced) was approximately 1–3 cm with a gradual boundary.

According to the CTD data, the temperature and salinity of bottom water in the study area of the Laptev Sea varied from -1.77 to -1.29°C and from 34.11 to 34.18 psu, respectively. Total alkalinity in near-bottom water was 2.3–2.5 mM.

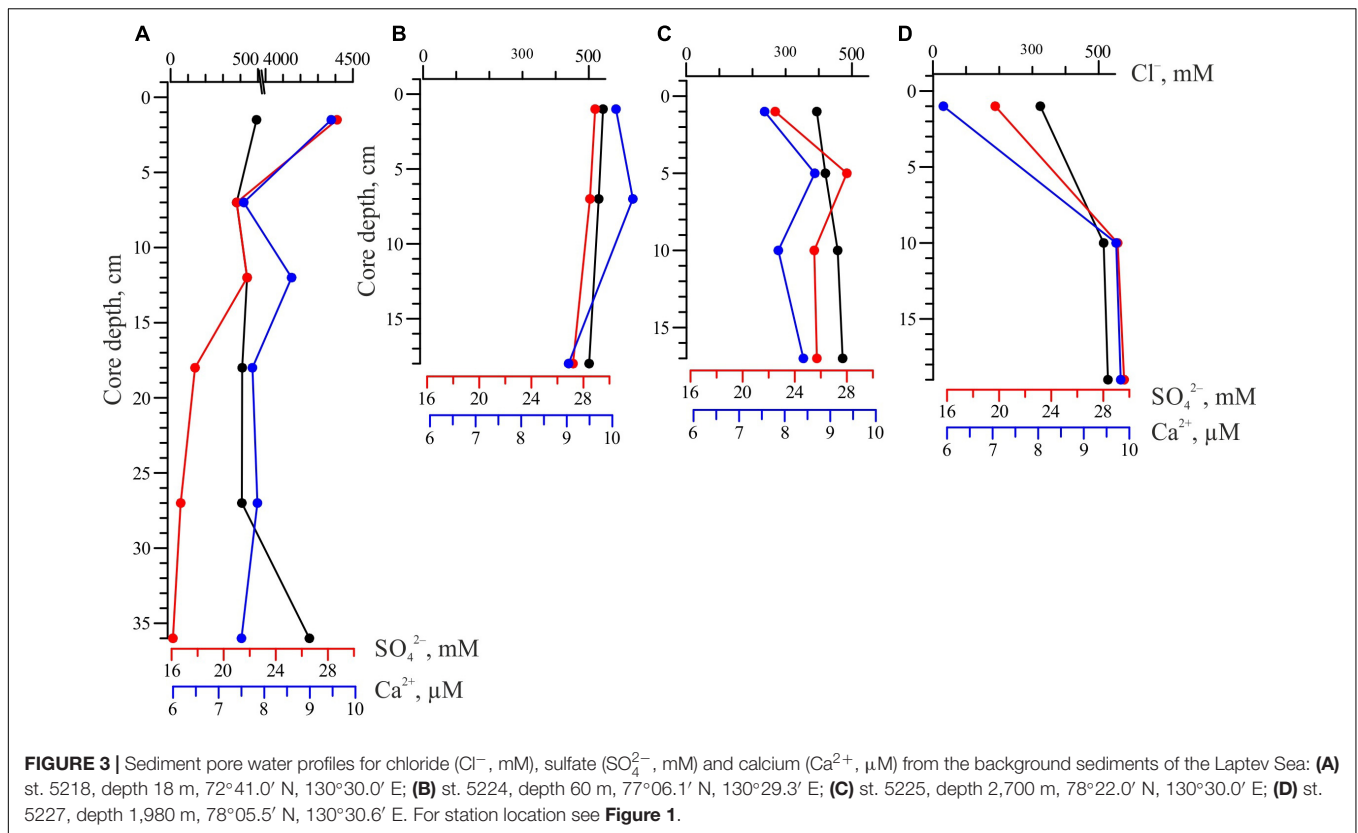
The pore water data from several cores collected at the seep area and adjacent areas are presented in **Figure 3**. There was a gradual increase in the Cl^- concentration, from 435 to 455 mM, in the surface sediment layer of the shelf background area within the depth changes from 18 m (St. 5218) to 60 m (St. 5224). These values are much lower than the Cl^- concentration in seawater

(558 mM). The Cl^- concentration in the pore water reached the lowest value (407 mM) in the seep area. The total alkalinity of the pore water within the seep area varied from 6.8 to 17.8 mM from the top to the bottom of the core.

The distinct influence of the sulfate reduction process (evident by SO_4^{2-} depletion from 24.8 to 16.0 mM) and an increase in total alkalinity (from 3.7 to 8.0 mM) in pore water was observed in the shallow-water area throughout the sampling sediment layer (St. 5218). The concentration of Ca^{2+} decreased from the top to the bottom of the cores from 9.5 to 7.5 μM . The lowest concentrations of Ca^{2+} are recorded in the surface sediment layer: 7.6 and 5.9 μM at stations 5225 and 5227, respectively.

Concentration and Isotopic Composition of Dissolved Methane in Bottom Sediments

Table 1 contains data on the dissolved methane concentration and carbon isotope composition of methane in the shelf sediments obtained at depths of 10–71 m. The concentrations of dissolved methane vary from 1 to 51 μM and locally reach to 539 μM in surface layer (0–10 cm) of bottom sediments



impacted by seepage. In the deeper sediment layer of 30–50 cm it concentrations range from 300 to 500 μM . Methane $\delta^{13}\text{C}$ values vary from -78.3 to -71.3‰ VPDB and indicate microbial origin of dissolved methane. CO_2 $\delta^{13}\text{C}$ values range from -24.4 to -16.3‰ VPDB. Methane oxidation resulted in formation of CO_2 .

The dissolved methane concentrations range from 0.03 to 0.09 μM in background bottom sediments of the shelf. The highest concentrations are characteristic of the inner shelf with a depth of about 20 m or less near the Lena Delta. Dissolved methane concentrations of about 0.02 μM are characteristic of the background bottom sediments of the continental slope with a depth of 1,500–2,400 m. CO_2 $\delta^{13}\text{C}$ values in background sediments range from -10.3 to -22.8‰ VPDB. Methane $\delta^{13}\text{C}$ values are absent due to too low concentration ($<0.01 \mu\text{M}$) of dissolved methane in background sediments (**Table 1**).

Carbonate Crusts

Petrography of Carbonates

Carbonates are highly porous, and cavernous carbonate-cemented crusts with a zonal distribution of gray and beige shades of colors. Focal zonality was confined to the burrows of tubeworms, biomorphic and detrital mineral inclusions, with hollow cavities and cavities containing sediments (**Figure 4**). Zonality is manifested in the textural structure and mineral composition. The crusts are dominated by calcite but exhibit mineralogical variability, characterized by focal enrichment in the Mg-carbonate phases.

Separate, relatively small carbonate crusts found during the washing out of the *Sigsbee* trawl and seafloor grab samples. They are represented by semi-rounded dense, porous, cavernous, carbonate-cemented crusts.

Carbonate crusts consist of a clastic terrigenous matrix of host sediments and micritic carbonate cement that is microcrystalline calcite precipitating within the host sediments. Clay-carbonate and carbonate-clay cements have a micrite (basal, microcrystalline) structure (**Supplementary Figure 2**). Their microtexture is very characteristic and is expressed in the development of structures of a rounded form (burrows of detritus feeders), composed of a substantially microgranular carbonate aggregate with a small amount of clastic material. The majority of the carbonate crusts had an uneven granular structure with micritic cement.

The internal structure of carbonate formations includes clastics and silt-sized matrices of different mineral compositions and roundness, cemented by carbonate and carbonate-clay. The clastic matrix (approximately 60–65%) consists of angular and semi-rounded grains ranging in size from 10 to 200 μm . The clastic grains are quartz, albite, microclines, pyroxene, amphibole, biotite, and ore minerals as accessories. The cement includes various fragments of organic residues and wood (**Supplementary Figure 3**).

Mineralogy of Carbonates

According to the XRD results, the carbonate contents of the crusts ranged from 8 to 60%. The cement was composed of

TABLE 1 | Dissolved methane concentration and stable carbon isotope composition ($\delta^{13}\text{C}$, ‰) of methane and carbon dioxide of the bottom sediments in the Laptev Sea.

Station number	Coordinates		Depth m	Layer cm	CH ₄ μM	$\delta^{13}\text{C}$ -CH ₄ ‰ VPDB	$\delta^{13}\text{C}$ -CO ₂ ‰ VPDB	Sampling tool
	N	E						
Sediments impacted by seepage								
5623*	76°53.65'	127°48.20'	63	0–1	1.41	-72.0	-	van Veen grab
5624	76°50.00'	126°39.88'	70	0–1	2.95	-78.3	-21.2	van Veen grab
5625	76°46.41'	125°49.40'	45	0–1	2.87	-77.4	-19.2	van Veen grab
				6–7	3.97	-76.6	-24.4	
5231*	76°46.34'	125°49.75'	71	0–1	19.2	-71.6	-2.8	Niemistö corer
				2–4	32.7	-74.8	-13.4	
				8–12	51.4	-68.3	-12.8	Niemistö corer
				4–5	12.7	-72.8	-	gravity corer
				10–11	9.9	-72.6	-14.4	
				37–38	385	-72.3	-12.0	
				44–45	467	-79.9	-6.8	
	1–4	539	-76.8	-	box corer			
Background sediments of shelf								
5228	77°39.00'	130°30.50'	87	0–2	0.046	-	-	Niemistö corer
				14–16	0.033	-	-	
5224	77°06.10'	130°29.30'	57	0–2	0.033	-	-	Niemistö corer
				15–17	0.041	-	-	
5223	76°28.20'	130°30.00'	56	0–2	0.038	-	-	Niemistö corer
				16–18	0.042	-	-	
5215	74°15.40'	130°30.50'	26	0–2	0.053	-	-16.0	Niemistö corer
				15–17	0.042	-	-10.4	
5220	73°20.30'	130°29.80'	25	0–3	0.090	-	-	Niemistö corer
				10–13	0.068	-	-	
5218	72°41.00'	130°30.00'	18	0–3	0.083	-	-11.3	Niemistö corer
				5–8	0.067	-	-10.5	
				22–25	0.075	-	-10.3	
Background sediments of continental slope								
5225	78°22.00'	130°30.00'	2385	0–2	0.019	-	-14.9	Niemistö corer
				9–11	0.023	-	-16.3	
				11–17	0.025	-	-22.8	
5226	77°49.30'	130°30.40'	1500	0–2	0.021	-	-	Niemistö corer
				2–5	0.025	-	-	

–, no data.

*, the host sediments of the authigenic carbonates.

authigenic Mg-calcite: up to 60 wt.% of the entire crystalline phase (mean 36 ± 11 wt. %, **Table 2**). Three main identifiable phases of this mineral can be distinguished with typical Mg contents of 2–23, 1–18, and 6–7 mol % MgCO₃ (**Table 2**). We distinguished the phases in those samples where Mg-calcite XRD peaks are reliably identified and do not overlap (**Supplementary Figure 4**).

Low-Mg calcite [1–2 mol % MgCO₃ according to Crémère et al. (2016b)] is present in minor quantities and represents the biogenic component which includes foraminiferal tests and calcite plates of unidentified species visible in smear slides (**Supplementary Table 1**).

Calcite, dolomite, and siderite clasts were identified within the silt sand-sized matrix cemented by Mg carbonate in the crust (sample OD-I-1). They occurred sporadically in trace amounts

(up to 4 wt. %). The re-deposited fine-grained calcite with a luminescent blue-white glow forms a vein on the surface of the crust with a calcite content of 56 wt. % and two phases of Mg-calcite of 12 and 32 wt. % (**Supplementary Table 1**, and **Supplementary Figure 5**). Calcite (100 wt. %) is present as bioclasts (colonial sea squirt) as well (**Supplementary Table 1**).

The detrital fraction of the carbonate crusts was represented by quartz, albite, anorthite, microcline, orthoclase, amphibole group minerals (hornblende), and mica (muscovite and biotite). The total content of clastic minerals in carbonate crusts (31–73 wt. %) is lower than in sediments (66–82 wt. %). In general, the composition of detrital minerals in the crusts is similar to that in the bottom sediments, but there are differences. Dark-colored monomineral fractions in the sediments are intergrowths and aggregates, in which the minerals of the amphibole group are the

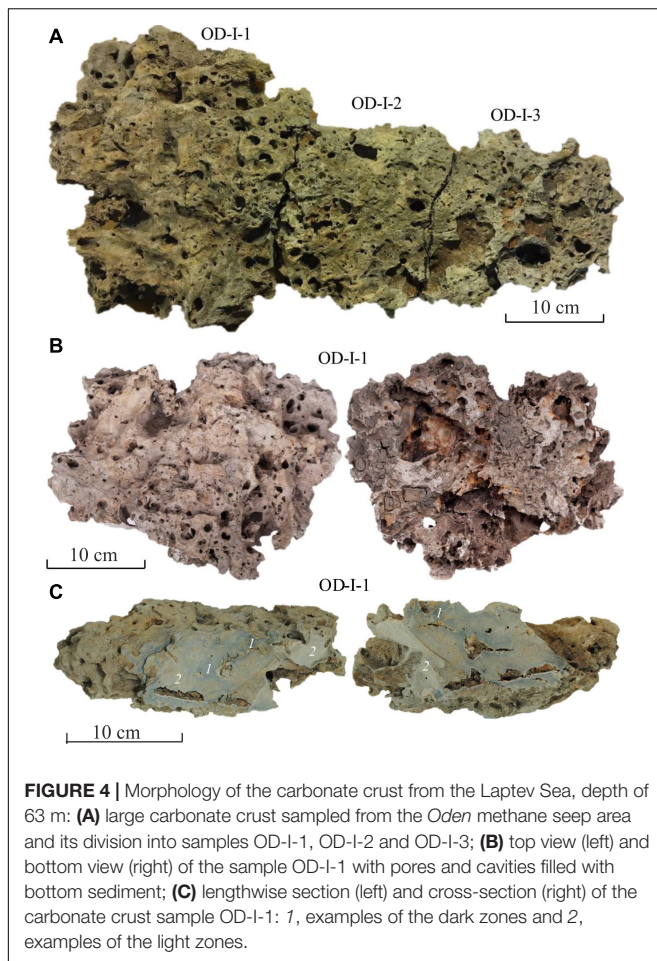


FIGURE 4 | Morphology of the carbonate crust from the Laptev Sea, depth of 63 m: **(A)** large carbonate crust sampled from the *Oden* methane seep area and its division into samples OD-I-1, OD-I-2 and OD-I-3; **(B)** top view (left) and bottom view (right) of the sample OD-I-1 with pores and cavities filled with bottom sediment; **(C)** lengthwise section (left) and cross-section (right) of the carbonate crust sample OD-I-1: 1, examples of the dark zones and 2, examples of the light zones.

main phase. However, the carbonate crusts were enriched with dark-colored tabular grains and debris of albite-biotite-quartz rock (**Supplementary Figure 6**).

The content of clay minerals (illite, smectite, kaolinite, and chlorite) in the crust samples varied from 7 to 23 wt. %. The ratio of clay minerals to Mg-calcite largely determines the color and texture of the crust. The darkest zones of the crusts were characterized by a decrease in the carbonate mineral content and an increase in the total content of clay minerals. This was due to an increase in the content of all clay minerals and the appearance of new mixed-layered (smectite-chlorite, illite-smectite) minerals characteristic of the darkest zones.

Separate burrows of detritus feeders with previously formed manganese hydroxides on the surface of the burrows were observed (**Supplementary Figure 3B**). According to the XRD data, this is a mineral with a weakly ordered crystal structure and strongest reflection with a d-spacing of 9.6 and 10 Å manganite, which corresponds to diagenetic todorokite (**Supplementary Table 1**).

Electron Microprobe Analysis of Carbonates

The microtexture of the carbonate crusts was clearly bioturbated, less often zonal, which generally appears along the burrows of detritus feeders. The micrite cement is represented by an

aggregate of Mg-calcite with clay minerals. There were areas composed of only Mg calcite. According to the SEM data, the admixture of Mg in calcite usually does not exceed 3 wt. %. Microstructural types of Mg-calcite can be distinguished as fine-grained (Mg 2–3 wt. %), forming the basis of carbonate cement (**Figure 5**); and clearly crystalline (Mg 1–2 wt. %).

Clearly, crystalline modifications of Mg-calcite fill the void spaces in the cement and burrows of detritus feeders. They also developed in the space between clastic minerals. The shapes of the crystals may differ and show signs of partial dissolution and recrystallization. Several forms were identified (**Figure 6**).

- (1) Scalenohedral crystals are the most common form of calcite that has already been encountered in the Laptev Sea (Kravchishina et al., 2017). Crystals ($\sim 30 \mu\text{m}$ along the axis) often form druses and twinning.
- (2) Fan-shaped crystals that form radial aggregates and druses. The length of the crystals along the axis is as large as 20–30 μm .
- (3) Rhombohedral crystals (up to 5 microns in size) usually develop along the first two types of calcite crystals and form aggregates.

Disulfide group minerals were formed in the structures during paragenesis with Mg-calcite. The main form of FeS_2 is marcasite (**Supplementary Figure 7**). Marcasite grows as inclusions (approximately 200–300 μm in diameter) within the dark stains of clay-rich micrite cement. Its crystals have a tabular shape and form radially positioned intergrowths with diameters of 5–10 μm . In contrast to the carbonate crusts, we observed only pyrite framboids in “host” sediments, while the above intergrowths were not found.

According to the XRD data, Mn hydroxide – todorokites were formed along the burrows of detritus feeders in association with Mg calcite (**Figure 6E** and **Supplementary Figure 8**). Evidently, these hydroxides are formed by the precipitation of Mn from a colloidal solution with the participation of microorganisms. These spherical formations (up to 5 μm in diameter) are often collected in chains or larger aggregates up to 20 μm in length, overlapping calcite crystals, and forming a continuous cover, which was black when examined under a microscope. The Mn content in these formations varied from 20 to 25 wt. %; Mg and Ca (at a 2–3 wt. %) are among the impurities with high X-ray intensity.

Major Element Composition of Carbonates and Bottom Sediments

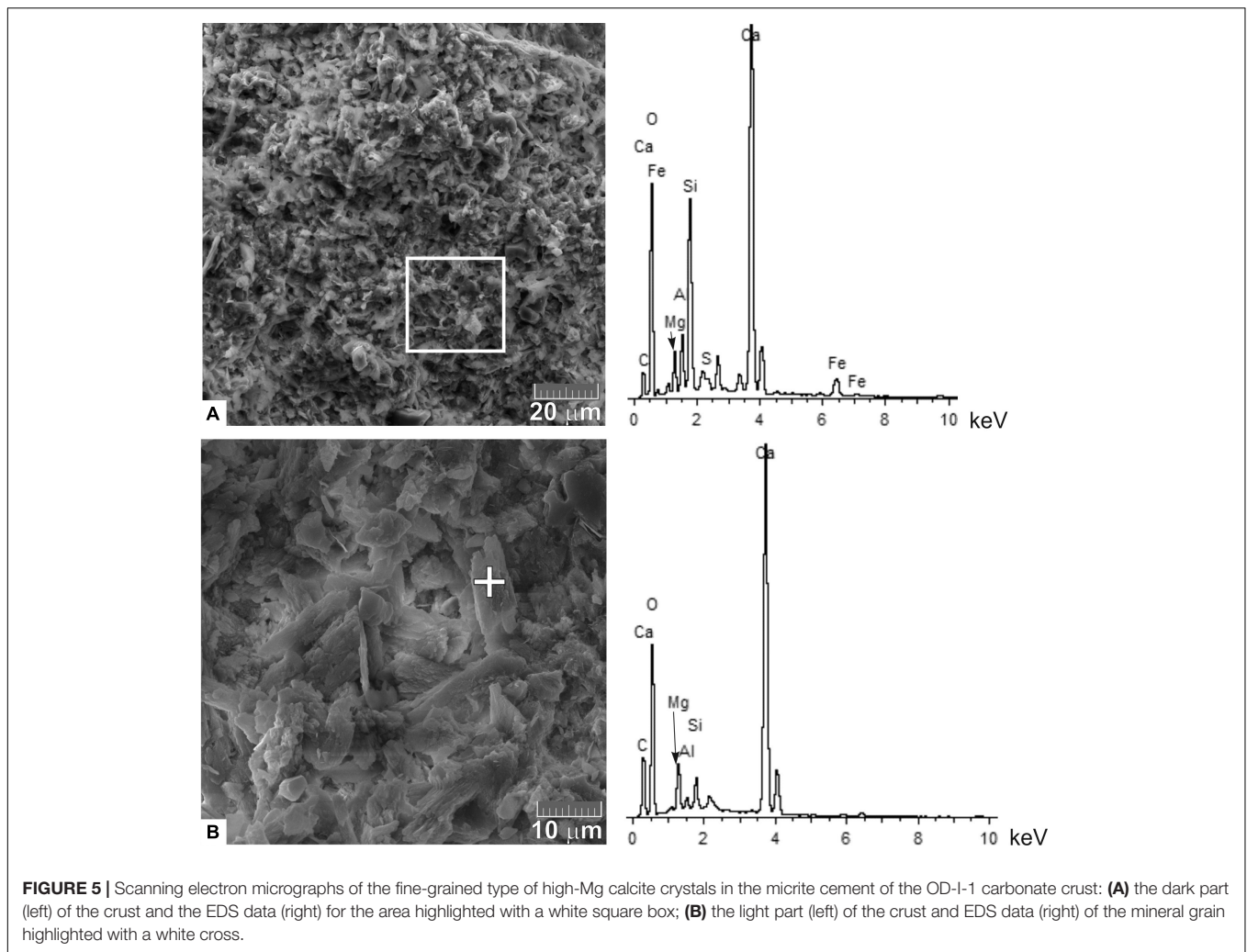
The XRF major element composition of the carbonate samples (especially in terms of carbonate-free matter) was significantly different from that of the surface layer of seafloor sediments (**Table 3**), collected near and at the *Oden* seep area. The sediments were composed of SiO_2 (56–72 wt. %).

Detrital contents in crusts, inferred from XRF data (**Table 3**), ranged between 38 and 72 wt. %, averaging at 49 ± 6 wt. %. The enrichment of the crusts with elements such as MgO , S_{tot} , and Sr (average 3.7 ± 0.3 wt. %, 0.7 ± 0.2 wt. %, and 1190 ± 114 ppm, respectively) associated with a carbonate material and marcasite was noticeable compared to the bottom sediments. The Sr/Ca

TABLE 2 | XRD mineral composition of the carbonate crust and bottom sediments from the *Oden* cold seep area.

Sample	Sub-sample	Quartz	K-feldspar	Plagioclase	Amphibole	Clinopyroxene	Smectite	Illite-smectite	Chlorite	Kaolinite	Dolomite		Calcite		Mg-calcites		
											wt. %	MgCO ₃ mol %	wt. %	MgCO ₃ mol %	wt. %	MgCO ₃ mol %	wt. %
Carbonate crust																	
OD-I-1	1	23	10	13	4			2	1		1						
	2	25	6	7	1			2	1								
	3	47	12	17	3			2	1		1						
	4	20	10	21	3			3	2			4					
	5	15	10	14	4			4									
	6	35	11	22	6			4									
	7	24	17	24	3			5	1		1	2					
	8	23	9	15	1			3			4						
	9	41	8	10	2			4	1		1						
	10	24	5	17	2		1	2	1		1						
	11	35	5	11	2		1	4	1		1						
	12	35	9	11	3		1	4	2		Traces						
	13	45	6	9	3		1	3	1		1						
	14	51	10	9	4		1	2	1		1						
	15	53	8	11	4		1	2	1		1						
	16	37	8	8	2		1	4	2		2						
	17	28	3	5	1		Traces	2	1		Traces						
	18	41	5	7	2		Traces	2	1		Traces						
OD-I-2	19	26	5	10	1			3	1		1	2					
	20	36	7	11	2			4	1		1						
	21	35	6	9	2			3	1		1						
	22	46	9	10	2			4	3		1	3					
	23 ¹	47	9	15	4		5	7	3		2	2					
	24	37	8	9	2			3	1		1	1					
Bottom sediments, surface layer (cm)																	
5623	0-1	34	15	26	3	3	4	8	3	2	1						
5624	0-2	25	12	24	4	1	5	10	10	4	1	1					
5625	0-1	36	13	26	3	4	4	8	4	2							

²³¹, bottom sediment sample from cavities of the carbonate crust OD-I-3.



ratio in the crusts varied in a narrow range from 0.005 to 0.008, which was controlled only by the contribution of Sr-rich Mg-calcite. Mg/Ca ratio in the studied samples of the crusts was constant and amounted to 0.1–0.2 indicating a relatively stable contribution of Mg-rich carbonate phase with minor input of Mg-low carbonate phase and detritus. The Mg/Ca ratio varied from 1.2 to 2.0 in the bottom sediments (including sediment samples collected from the pores and cavities of the crusts – 1.4).

In contrast, the carbonate crusts were deficient in trace elements such as V, Zn, Rb, Zr, Ba, and Pb (average content 41 ± 7.3 , 28 ± 4.1 , 56 ± 5.1 , 90 ± 30 , 353 ± 43 , and <10 ppm, respectively, **Table 4**) compared to the bottom sediment. The titanium modulus of TiO_2/Al_2O_3 was 0.04–0.06 and 0.06–0.07 in the bottom sediments and in the carbonates, respectively. The alkaline modulus of Na_2O/K_2O was 0.6–1.0 in the carbonate crusts. It varied from 1.0 to 1.3 in the bottom sediments, indicating a higher admixture of plagioclases.

Oxygen Isotope Composition of Carbonates

The $\delta^{18}O$ values of carbonate fragments of crusts range from 3.7 to 4.8‰ VPDB with the average is 4.4 ± 0.2 ‰

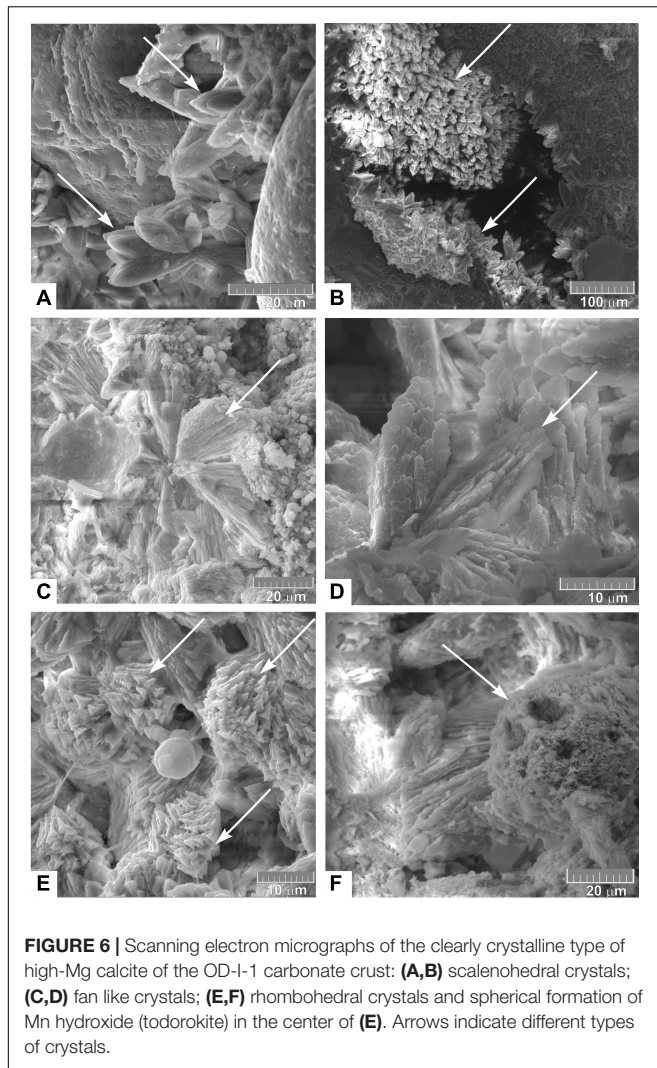
VPDB, $n = 11$, **Table 5**. This range corresponds to the low-temperature precipitation of carbonates from seawater. This range corresponds to the low-temperature precipitation of carbonates from the ambient seawater ($\delta^{18}O$ range from –0.2 to –0.5‰ VSMOW, unpublished data). The eq. (1) for Mg-calcite and water can be derived as weighted average fractionation factor for magnesite and calcite:

$$\alpha(Mg - Cc - Water) = x \cdot \alpha(Magnesite - Water) + (1 - x) \cdot \alpha(Calcite - Water) \quad (1)$$

We used the eqs. (2, 3) of Chacko and Deines (2008) obtained for low-T interval (0–130°C) closest to observed CTD data (–1.77°C):

$$\alpha(Mgs - Water) = 2.388 \cdot 10^6(T^{-2}) + 9.212 \cdot 10^3(T^{-1}) - 17.792 \quad (2)$$

$$\alpha(Cc - Water) = 1.692 \cdot 10^6(T^{-2}) + 7.649 \cdot 10^3(T^{-1}) - 16.925 \quad (3)$$



where x – is the mole part of MgCO_3 in calcite and T is temperature in Kelvin.

It is important that at low temperatures the difference between the $\alpha(\text{Cc-Water})$ and $\alpha(\text{Mgs-Water})$ is significant. So, for the Mg-calcite with the 2% of MgCO_3 the $\delta^{18}\text{O}$ value of the Mg-calcite equilibrated with the ambient seawater should be range from +3.07 to +3.36‰ VPDB while for the Mg-calcite with the 20% of MgCO_3 the $\delta^{18}\text{O}$ value should be range from +5.57 to +5.86‰ VPDB. The obtained ranges of $\delta^{18}\text{O}$ from +3.7 to +4.8‰ VPDB can be referred to mean MgCO_3 content no more that 4–14%. The $\delta^{18}\text{O}$ value of sediments from the cavity in the carbonate crust is significantly less (–4.1‰ VPDB) and shows non equilibrium relations with the surrounding seawater.

Carbon Isotope Signatures of Carbonates and Carbon Content

The CaCO_3 content in the carbonates ranged from 45 to 61 wt. % (Table 6). The C_{org} content of 0.4–0.5 wt. % characterized the upper layer (0–13 cm) of sediments collected from the inner part of the zone where the trawl sample with carbonates was obtained

(st. 5623). The C_{org} content in the crusts was 0.2–0.3 wt. %, rarely rising to 0.4 wt. % within the gray zone, which was enriched in clay minerals and depleted in authigenic carbonates (Table 4).

The $\delta^{13}\text{C-C}_{\text{org}}$ values of sediments lie within limits characteristic of terrigenous (allochthonous) organic matter (OM); on average, the $\delta^{13}\text{C-C}_{\text{org}}$ was -27.7 ± 1.5 ‰ VPDB (Table 6). The carbon isotope composition of OM in the carbonate crusts was significantly depleted in heavy isotopes compared to the OM in the sediments (average of -34.6 ± 2.2 ‰ VPDB). This suggests the participation of methane-derived carbon in the formation of OM in the carbonate crusts. Methane-derived carbon is also involved in the formation of ^{13}C -depleted inorganic carbon in carbonates showing values between –27.9 and –34.8‰ VPDB (Tables 5, 6). This is particularly apparent from the example of small crusts with smaller clay mineral contents ($\delta^{13}\text{C-CaCO}_3$ up to –40.2‰ VPDB) (Table 5).

DISCUSSION

The studied carbonate crusts are nearly monomineral carbonate phases and detrital materials. On average, carbonate structures consist of Mg-calcite (inferred from XRD data up to 55%). Their carbonate cement is composed mostly of high-Mg calcite (up to 23 mol % MgCO_3). Low-Mg calcite re-deposited minerals sometimes form single crystals in the form of thin anisotropic plates (<0.1 mm) sunk in carbonate cement.

The carbonate crusts of cold seeps usually comprise a mixture of different minerals (e.g., aragonite, high-Mg calcite, and calcite) (Bayon et al., 2007). The studied carbonate crusts varied from those found at the sediment surface in the Northern, Norwegian, and Barents Seas (Crémière et al., 2016a,b; Mazzini et al., 2016; Sauer et al., 2017). Several carbonate phases, not only Mg calcite, were identified. Aragonite was absent in the studied carbonate crusts, probably due to the low concentration of SO_4^{2-} and high dissolved sulfide concentration in the pore water that can inhibit the precipitation of aragonite, favoring Mg^{2+} incorporation into the calcitic structure (Zhang et al., 2010, 2012) and the precipitation of high-Mg calcite versus aragonite (Lu et al., 2018). In addition, it is possible that carbonate cementation of methane-charged sediment did not occur near the sediment-water interface, but in the sediment layer, that is, at a depth with an expected low concentration of SO_4^{2-} and lower AOM rate (Lein et al., 1999; Whiticar, 1999; Aloisi et al., 2002; Valentine, 2002). Carbonate crusts formed by Mg-calcite probably reflect a formation deeper in the sediment column under higher H_2S conditions (Whiticar, 1999; Aloisi et al., 2002; Crémière et al., 2016b). Total dissolved sulfide concentration in pore water of studied subsurface sediments was up to 400 μM (Savvichev et al., 2018a). The metabolism of sulfate-reducing bacteria may create a local environment with elevated concentration of dissolved sulfide, which may favor the precipitation of high-Mg calcite (Valentine and Reeburgh, 2000; Peckmann et al., 2001; Zhang et al., 2010, 2012; Lu et al., 2018; Smrzka et al., 2021). Active sulfate reduction occurred everywhere in bottom sediments of the studied seepage area but the highest sulfate reduction rate (2240–4865 $\text{nM S dm}^{-3} \text{ day}^{-1}$) was found in

TABLE 3 | XRF major element composition of the carbonate crust and sediment samples.

Sample	Sub-sample	LOI	Na ₂ O	MgO	Al ₂ O ₃	SiO ₂	K ₂ O	CaO	TiO ₂	MnO	Fe ₂ O _{3tot}	P ₂ O ₅	S _{tot}	Total	Detrital content
%															
Carbonate crusts															
OD-I-1	1	20.71	1.04	4.08	6.23	37.23	1.43	25.12	0.39	0.21	2.63	0.22	0.22	99.51	47.9
	2	22.85	0.95	4.16	5.39	33.43	1.24	28.02	0.33	0.20	2.35	0.26	0.28	99.46	42.7
	3	19.69	1.16	3.32	5.36	41.63	1.35	24.13	0.30	0.16	2.02	0.18	0.22	99.52	50.7
	4	19.35	1.07	3.98	6.51	39.55	1.46	23.79	0.40	0.17	2.66	0.23	0.28	99.45	50.6
	5	20.86	1.11	3.49	6.41	39.55	1.41	22.48	0.41	0.26	2.90	0.22	0.32	99.42	50.7
	6	23.78	1.01	3.60	5.18	33.91	1.21	27.30	0.31	0.20	2.24	0.23	0.38	99.35	42.9
	7	11.22	1.57	2.50	8.17	57.50	1.83	11.87	0.47	0.15	3.61	0.14	0.36	99.39	71.6
	8	21.74	1.13	3.23	6.20	40.74	1.38	21.06	0.39	0.22	2.90	0.19	0.28	99.46	51.6
	9	19.81	1.13	3.60	5.58	40.76	1.30	24.28	0.31	0.18	2.06	0.23	0.24	99.48	50.0
	10	18.86	1.09	3.74	6.17	41.69	1.40	23.04	0.37	0.23	2.48	0.21	0.23	99.51	52.1
	11	21.37	1.06	3.90	5.78	36.09	1.29	26.02	0.38	0.31	2.49	0.24	0.40	99.33	46.0
	12	20.55	1.00	3.89	6.49	39.07	1.42	23.03	0.42	0.19	3.10	0.21	0.19	99.56	50.5
	13	22.56	1.02	4.44	5.71	34.18	1.20	26.77	0.35	0.13	2.44	0.24	0.35	99.39	43.9
	14	14.11	1.47	3.51	6.54	51.08	1.50	18.42	0.37	0.09	2.10	0.18	0.18	99.55	61.6
	15	13.09	1.55	3.49	7.31	52.24	1.64	16.81	0.44	0.13	2.58	0.18	0.14	99.60	64.2
	16	18.63	1.24	4.07	6.91	41.37	1.44	21.61	0.42	0.19	3.14	0.23	0.24	99.49	53.3
	17	22.74	1.17	4.37	5.01	33.84	1.10	28.39	0.28	0.13	1.89	0.22	0.29	99.43	42.1
	18	20.21	1.22	3.97	5.57	38.66	1.24	24.20	0.41	0.14	2.56	0.21	0.67	99.06	48.4
OD-I-2	19	22.61	0.96	3.53	6.69	26.75	1.40	33.45	0.45	0.23	2.89	0.30	0.49	99.75	38.2
	20	18.57	0.98	3.61	7.48	30.92	1.63	31.75	0.52	0.25	3.12	0.34	0.57	99.74	43.7
	21	19.77	1.03	3.61	7.67	30.83	1.61	30.19	0.48	0.21	3.41	0.37	0.55	99.73	44.0
OD-I-3	22	19.45	1.01	3.56	7.20	30.00	1.55	31.95	0.49	0.16	3.13	0.37	0.85	99.72	42.4
	23 ¹	4.51	1.64	2.05	14.86	64.98	3.09	1.48	0.80	0.06	5.65	0.14	0.49	99.75	89.4
	24	20.70	0.95	3.73	6.86	28.70	1.50	32.67	0.45	0.15	2.77	0.36	0.87	99.71	40.3
Bottom sediments															
5623	0–1	3.38	3.20	1.67	11.58	71.67	2.52	1.39	0.43	0.21	3.32	0.15	0.26	99.78	89.5
5624	0–1	10.45	2.39	2.89	14.34	56.57	2.48	1.47	0.76	0.32	7.49	0.21	0.38	99.75	81.6
	1–2	6.84	3.98	2.52	15.26	55.71	2.76	1.75	0.85	0.25	8.87	0.17	0.39	99.35	83.5
5625	0–1	6.61	2.79	2.54	13.84	62.55	2.57	1.48	0.69	0.19	5.96	0.20	0.32	99.74	85.6
	1–2	6.67	2.75	2.54	14.12	62.84	2.64	1.45	0.69	0.09	5.71	0.18	0.26	99.94	86.0

23¹, bottom sediment sample from cavities of the carbonate crust.

the subsurface reduced sediments where methane oxidation rate were high (Savichev et al., 2018a). This is an indication of sulfate-dependent AOM. MDACs are usually formed in subsurface sediments at cold seeps due to AOM, resulting from the microbial oxidation of methane-rich fluids (Paull et al., 1984; Bohrmann et al., 1998; Aloisi et al., 2002; Bayon et al., 2009; Mazzini et al., 2016). For example, modern carbonate formation with the participation of methane carbon was identified earlier in sub-surface Holocene sediments of the Laptev Sea shelf within the studied cold seep area (Kravchishina et al., 2017). However, the texture and mineralogy of the studied carbonates differed significantly from those collected in the sub-surface sediment.

The micritic carbonate cements display similar major composition patterns, regardless of their mineralogy. The background sediments are predominantly clayey and contain little carbonates (1–2%), or none at all. The clastic material in host marine sediments differs significantly compared to clastic material within the carbonate crusts (Figure 7). Generally, the crust material is less alkaline, depleted of titanium and iron, but

enriched chromium and vanadium in comparison with surface bottom sediments (Figure 8). The horizontal-crust variation of major and some trace element compositions reflect the relative contributions of Mg-rich carbonate phases and detrital material from different sources. XRF major element composition and XRD of the carbonate samples and bottom sediments suggest that the carbonate cementation of the detrital components occurred not on the seafloor surface of the studied area and that they were possibly relocated from deeper layers of sediment. We believe that winnowing is the most possible mechanism of carbonate exposure (Peckmann and Thiel, 2004; Smrzka et al., 2019).

The newly discovered carbonate crusts are authigenic. The concept “authigenic mineral” implies that it is formed *in situ* within the depositional site in response to geochemical processes. The studied carbonates, strictly speaking, cannot be attributed to the “formed in place” formations. In our case, the binding of authigenic carbonates to a specific sediment type was not obvious. It is not known where exactly carbonate precipitation occurred in sediments because the formation of carbonate hard pavements

TABLE 4 | XRF trace element composition of the carbonate crust and sediment samples.

Sample	Sub-sample	Cr	V	Co	Ni	Cu	Zn	Rb	Sr	Zr	Ba	U	Th	Y	Nb	Pb
Ppm																
Carbonate crusts																
OD-I-1	1	17	41	11	26	17	29	54	1136	75	350	<5	6	19	10	<10
	2	23	32	11	24	11	24	48	1266	65	300	<5	<5	18	11	<10
	3	14	30	<10	19	<10	20	50	1163	83	367	<5	<5	18	<10	<10
	4	25	39	<10	30	<10	29	57	1107	82	353	<5	5	21	11	<10
	5	25	34	14	30	11	32	57	1051	91	339	<5	5	20	11	<10
	6	20	30	<10	18	<10	23	47	1249	57	310	<5	5	16	<10	<10
	7	38	78	14	29	11	37	78	654	190	529	<5	<5	20	12	<10
	8	23	47	<10	29	14	32	55	1053	95	333	<5	6	20	11	<10
	9	17	39	10	21	<10	23	50	1186	78	363	<5	<5	19	10	<10
	10	12	41	10	23	<10	26	56	1068	80	349	<5	<5	18	<10	<10
	11	23	37	12	28	<10	27	52	1186	73	335	<5	<5	19	12	<10
	12	28	49	13	29	16	35	59	1052	76	324	<5	<5	22	11	<10
	13	23	31	<10	25	10	27	50	1206	55	314	<5	<5	15	10	<10
	14	29	35	<10	17	85	24	61	907	140	461	<5	5	15	11	<10
	15	36	47	<10	18	<10	30	66	778	184	490	<5	9	20	12	<10
	16	30	53	13	26	11	36	62	981	108	391	<5	<5	20	12	<10
	17	13	35	12	16	<10	22	45	1315	62	316	<5	6	16	<10	<10
	18	30	30	6	17	<10	23	52	1104	164	368	<5	8	18	11	<10
OD-I-2	19	59	44	<10	45	16	30	56	1180	56	264	<5	6	18	9	<10
	20	34	47	10	35	<10	30	63	1084	64	326	<5	5	21	10	<10
	21	32	48	13	32	20	34	61	1157	62	324	<5	5	26	11	<10
OD-I-3	22	22	40	6	29	22	27	56	1199	65	294	<5	5	18	12	<10
	23 ¹	91	175	12	47	14	58	110	317	186	523	<5	9	34	12	26
	24	29	39	11	28	38	34	57	1330	57	334	<5	6	23	<10	<10
Bottom sediments																
5623	0-1	49	118	13	22	11	47	100	271	212	683	<5	6	24	10	15
5624	0-1	111	257	23	67	28	115	124	217	198	512	<5	16	37	17	37
	1-2	158	310	31	97	33	140	159	287	224	604	<5	12	53	18	56
5625	0-1	101	215	18	45	22	87	114	252	310	558	<5	12	35	12	31
	1-2	98	220	18	43	21	92	118	243	302	603	<5	14	33	14	34

23¹, bottom sediment sample from cavities of the carbonate crust.

and crusts cannot occur at the water/sediment interface in the modern shallow Eurasian Arctic shelf. The studied carbonates would nonetheless be authigenic, i.e., formed within the sediment in response to hydrocarbon-rich fluid seepage and microbial processes. The surface layers of the studied sediments were typical of the Laptev Sea outer shelf (Nürnberg et al., 1995), weakly carbonated (<3% CaCO₃), terrigenous (quartz and aluminosilicates predominate), and soft muds with an oxidized surface layer. It is well known that high-latitude oceans have lower pH naturally, calcium carbonate mineral saturation states, and buffering capacity because of the higher solubility of CO₂ in their cold waters, and experience undersaturation for calcium carbonate minerals (Bates et al., 2009). The shallow Arctic shelf seas are known to be especially corrosive to carbonate precipitation (Yamamoto-Kawai et al., 2009, 2016; Semiletov et al., 2016). Furthermore, aerobic oxidation of methane at the water/sediment interface results in an increase in acidity, favoring carbonate dissolution (Reeburgh, 2007). Therefore, the primary goal of the study of carbonate crusts at 76°53' N

and 127°48' E in the Laptev Sea was to reveal the origin of authigenic carbonate pavements on the seafloor of the *Oden* cold seep area.

Our results show a difference between the cold seep field and background pore water Cl⁻ and SO₄²⁻ concentrations. The Cl⁻ concentration supports the conclusion that there is a sign of low-salinity pore fluids flowing through sediments, which possibly indicating dissociation of permafrost-associated gas hydrates (e.g., Romanovskii et al., 2006; Semiletov et al., 2012). Numerous methane seeps and microbial mats associated with seeps have been found in the study area (Shakhova et al., 2015; Savvichev et al., 2018a; Baranov et al., 2020; Vedenin et al., 2020). The GHSZ and the permafrost layer can disintegrate though with possible diffuse emissions. The size of the Arctic subsea intrapermafrost gas hydrates reservoir, its spatial distribution, as well as its biogeochemical and physical characteristics remain poorly known (Puglini et al., 2020). Modern faults found on the Laptev Sea shelf can serve as supply channels for vertical fluid flow (Rekant and Gusev, 2009). The studied methane seep field

TABLE 5 | Stable carbon and oxygen isotope composition of the crusts.

Sample	Sub-sample	$\delta^{13}\text{C}$	$\delta^{18}\text{O}$
		%‰ VPDB	
Carbonate crust			
OD-I-2	19	-34.3	4.8
	20	-33.8	4.5
	20 ²	-33.8	4.1
	21	-29.9	4.7
	21 ²	-29.9	4.2
OD-I-3	22	-29.9	4.5
	22 ²	-30.2	4.1
	23 ¹	-21.3	-4.1
	23 ^{1,2}	-21.2	-7.7
	24	-29.2	4.5
	24 ²	-28.9	3.8
Small carbonate crusts			
OD-1	1	-36.8	4.5
	1 ²	-35.9	4.1
OD-2	2	-36.3	4.5
	2 ²	-36.2	4.3
OD-3	3	-30.3	4.7
	3 ²	-30.4	3.9
OD-4	4	-35.1	3.6
	4 ²	-32.1	1.8
OD-5	5	-34.8	4.2
	5 ²	-35.1	4.0
OD-6	6	-40.2	4.3
	6 ²	-40.1	3.7

¹Bottom sediment sample from cavities of the crust.

²Samples treated with H₂O₂ to assess the influence of organic matter impurities.

is linked to a fault system consisting of deep-seated and surface faults. Taliks and areas of fault zones (where geothermal heat flux is the greatest) provide possible gas migration pathways by which CH₄ can be released from seabed deposits to the water column. The deep-seated faults belonging to the Laptev Sea Rift System and the KLFZ serve as conduits for gas migration from the lower sediment strata to the gas reservoir in the upper sediment strata below the caprock formed by permafrost and gas hydrates. Shallow faults related to the subsidence of the outer shelf cut this caprock and form conduits for intense bubble methane discharge observed within the studied seep field. A 3D graphical model of the Laptev Sea slope and shelf with faults that may serve as conduits for thermogenic methane migration and emission was presented in the article by Baranov et al. (2020). The gas reservoir possibly lies beneath the GHSZ and the permafrost layer. The direct confirmation of the hypothesis of thermogenic methane seepage associated with fault–gas reservoir system in the Laptev Sea is not possible at present because no deep wells have yet been drilled. However, thermally generated gas which has probably migrated upward from deeper sedimentary strata was detected among gaseous hydrocarbons adsorbed in near-surface sediments at the northern margin of the shelf (Cramer and Franke, 2005) close to our studied area.

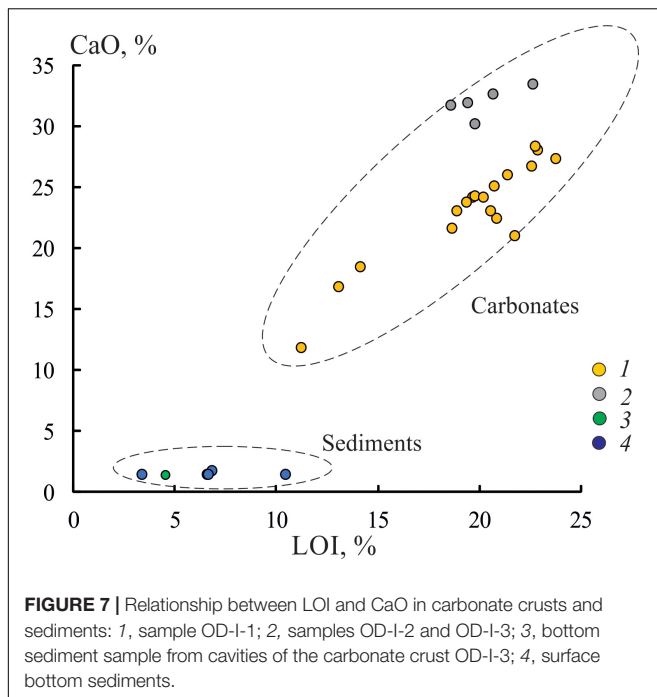
TABLE 6 | Content of organic and inorganic carbon calculated as CaCO₃ and stable carbon isotope composition of carbonate crust.

Sample	Sub-sample	C _{org}	CaCO ₃	$\delta^{13}\text{C-C}_{\text{org}}$	$\delta^{13}\text{C-CaCO}_3$
		wt. %		%‰ VPDB	
Carbonate crust					
OD-I-1	1	0.31	49.8	-34.9	-30.1
	2	0.38	58.5	-37.2	-33.1
	3	0.27	51.5	-40.2	-30.5
	4	0.25	50.2	-31.2	-34.8
	5	0.32	52.0	-31.1	-25.9
	6	0.31	60.9	-35.1	-31.4
	7	0.44	26.6	-32.7	-30.2
	8	0.34	43.6	-34.7	-27.9
	9	0.31	57.2	-	-36.8
	10	0.33	58.0	-	-33.9
	11	0.29	56.5	-	-36.8
	12	0.26	58.2	-	-35.6
	13	0.32	56.5	-	-37.5
	14	0.40	49.6	-	-28.9
	15	0.28	43.2	-	-25.6
	16	0.30	43.9	-	-29.9
	17	0.45	49.0	-	-29.0
	18	0.33	48.7	-	-29.4
Bottom sediments, layers in cm					
5623	0–1	0.51	1.47	-30.5	-7.0
	1–3	0.49	0.17	-28.2	-6.1
	3–13	0.41	0.02	-23.5	-6.3
5624	0–2	1.09	2.59	-28.5	-9.1
	2–6	1.06	1.18	-30.2	-2.1
	6–14	0.9	1.27	-27.7	-2.9
5625	0–0.5	0.65	1.0	-27.1	-6.1
	0.5–13	0.75	0.9	-25.8	-3.5
	0–1	0.62	0.5	-27.6	-5.0

–, no data.

The dissolved CH₄ concentrations of surface sediments varied from 1–2 to 3–539 μM depending on the redox conditions. The highest CH₄ concentration was found in the sediments inhabited by symbiotrophic siboglinidae and thyasirid bivalves (Savvichev et al., 2018a; Vedenin et al., 2020). These values were greater than the range of typical concentrations for oxidative (0.01–2.00 μM) and reducing (2.5–13.0 μM, less often up to 20 μM) sediments of the Laptev Sea (Savvichev et al., 2010, 2018b; Lein et al., 2013). The mats of methanotrophic bacteria were characterized, and active microbial methane oxidation was determined in the upper sediment layer within the cold seep area. Both aerobic methanotrophic bacteria and anaerobic consortium activity contributed to this process (Savvichev et al., 2018a). Unconsumed CH₄ diffused into the near-bottom water, where it was actively oxidized by methanotrophic water bacteria forming the second microbial biofilter.

The observed low $\delta^{13}\text{C}$ values of dissolved CH₄ (from -68.3 to -79.9‰ VPDB, **Table 1**) indicated its microbial origin in the sediments. Typically, methane is weakly generated by microorganisms in sediments of the Siberian shelf seas with low



C_{org} content (often $<0.5\%$), e.g., the rate of methanogenesis in the outer shelf surface sediments of the Kara Sea was $2.1\text{--}3.5\text{ nM CH}_4\cdot\text{dm}^{-3}\cdot\text{day}^{-1}$ (Savvichev et al., 2010) and of the Chukchi Sea was $0.8\text{--}1.8\text{ nM CH}_4\cdot\text{dm}^{-3}\cdot\text{day}^{-1}$ (Lein et al., 2007). Low rates of methanogenesis in sediment samples from the seeping area (from 4 to $53\text{ nM CH}_4\cdot\text{dm}^{-3}\cdot\text{day}^{-1}$, Savvichev et al., 2018a) indicated that high dissolved CH_4 concentrations and high rates of methane oxidation were caused by methane flow from deeper sediment strata. To generate carbonates through the AOM turnover additional participation of dissolved CH_4 is required and therefore additional sources of methane are expected. The primary sources highlighted above can include: (i) dissociation of intrapermafrost gas hydrates; (ii) methane flow from the thawing of relict subsea permafrost; (iii) thermally generated methane-rich fluids related to gas reservoir. Considering the fact that the subsea permafrost is possibly absent on the outer Laptev Sea shelf (Cramer and Franke, 2005; Baranov et al., 2020), the upward migration of thermogenic methane is the most appropriate alternative source. We hypothesize that, bubble methane appears to have a heavier isotopic composition compared with studied dissolved methane, and should include a thermogenic, not only microbial source. Because methane in marine sediments may produce not only by microbial but thermal degradation of organic carbon often linked to offshore hydrocarbon reservoirs (Milkov et al., 2003) as shown for the Laptev Sea shelf (Cramer and Franke, 2005). The flow of thermogenic methane-rich fluids through fault zones typically captures microbial methane from sediments (Whiticar, 1999; Naehr et al., 2007; Milkov and Etiope, 2018). Therefore, in the studied area, the methane that participated in the formation of carbonates could be both microbial and thermogenic.

The C_{org} of sediments in the studied area was depleted in the ^{13}C isotope ($\delta^{13}\text{C}\text{-}C_{org}$ varied from -30.5 to -23.5% VPDB), which implies the prevalence of terrigenous OM. The terrestrial OM is commonly considered to be more resistant to microbial degradation (Hedges and Mann, 1979; Tesi et al., 2014). The predominance of terrigenous OM versus marine OM inhibits the microbial processes of OM decomposition in the bottom sediments of Siberian shelf and, as a result, may prevent the transition from heterotrophic to symbiotrophic types of nutrition (Lein, 1984; Lein et al., 1996). Although a non-conservative behavior of terrestrial organic compounds buried in Laptev Sea shelf sediment have shown in several studies (Semiletov et al., 2013; Tesi et al., 2014). Terrigenous OM mineralization occurs largely by bacterial sulfate reduction (Brüchert et al., 2018). The biogeochemical fate of terrigenous OM deposited on the Arctic shelf is still one of the most important open questions for the marine Arctic carbon cycle (e.g., Tesi et al., 2014; Macdonald et al., 2015; Brüchert et al., 2018).

The OM extracted from the studied carbonate crusts ($\delta^{13}\text{C}\text{-}C_{org}$ from -40.2 to -31.1% VPDB) is depleted in isotopically heavy C_{org} , compared to the “host” sediments because AOM strongly discriminate against methane containing the heavy isotope ^{13}C (Peckmann and Thiel, 2004; Peckmann et al., 2009). It can be a result of capture of methanotrophic bacterial biomass at the time of carbonate precipitation and their incorporation into microcrystalline carbonate matrix (Marlow et al., 2014; Yao et al., 2021), which is typical for seep carbonates and known Arctic MDACs as well (Pauly, 1963; Schubert et al., 1997; Lein et al., 1999; Kravchishina et al., 2017). Methane oxidation resulted in formation of bicarbonate and OM (both as microbial biomass and as soluble extracellular secretions). Therefore ^{13}C -depleted C_{org} of seep carbonates is diagnostic for bacteria mediating oxidation of methane (Yao et al., 2021).

According to the $\delta^{13}\text{C}$ values of carbonate crusts studied we can conclude that the microbial methane was a main source of carbon for their formation. Indeed, the fractionation factor of carbon isotopes at low temperatures is high. For example, at water temperature of 4°C the value of $10^3\ln\alpha(\text{CO}_2\text{-CH}_4)$ can vary from 76.9% (Horita, 2001) to 76.1% (Bottinga, 1969). Using these fractionation factors one can estimate that the $\delta^{13}\text{C}$ value of methane equilibrated with the studied carbonates should be approximately from -98 to -117% VPDB. The $\delta^{13}\text{C}$ values of dissolved methane from the bottom sediments of studied area are significantly higher (from -71 to -78% VPDB, **Table 1**) than the calculated $\delta^{13}\text{C}$ values of the methane in equilibrium with carbonate of studied crusts. This indicates that the dominant methane source during carbonate crust formation and in modern “host” sediments is changed.

The process of AOM in modern sediments of studied area can be illustrated by the relations between $\delta^{13}\text{C}\text{-CO}_2$ and $\delta^{13}\text{C}\text{-CH}_4$ values of dissolve gasses (**Table 1**). The difference between these δ -values does not correspond to low-temperature isotope equilibrium between methane and carbon dioxide. Only in deepest sample studied (st. 5231, layer 44–45 cm) the $\Delta^{13}\text{C}(\text{CO}_2\text{-CH}_4)$ value may correspond to equilibrium at 13°C according to the equation of Horita (2001) or 11°C according to the equation of Bottinga (1969). Estimates the temperature for other samples in

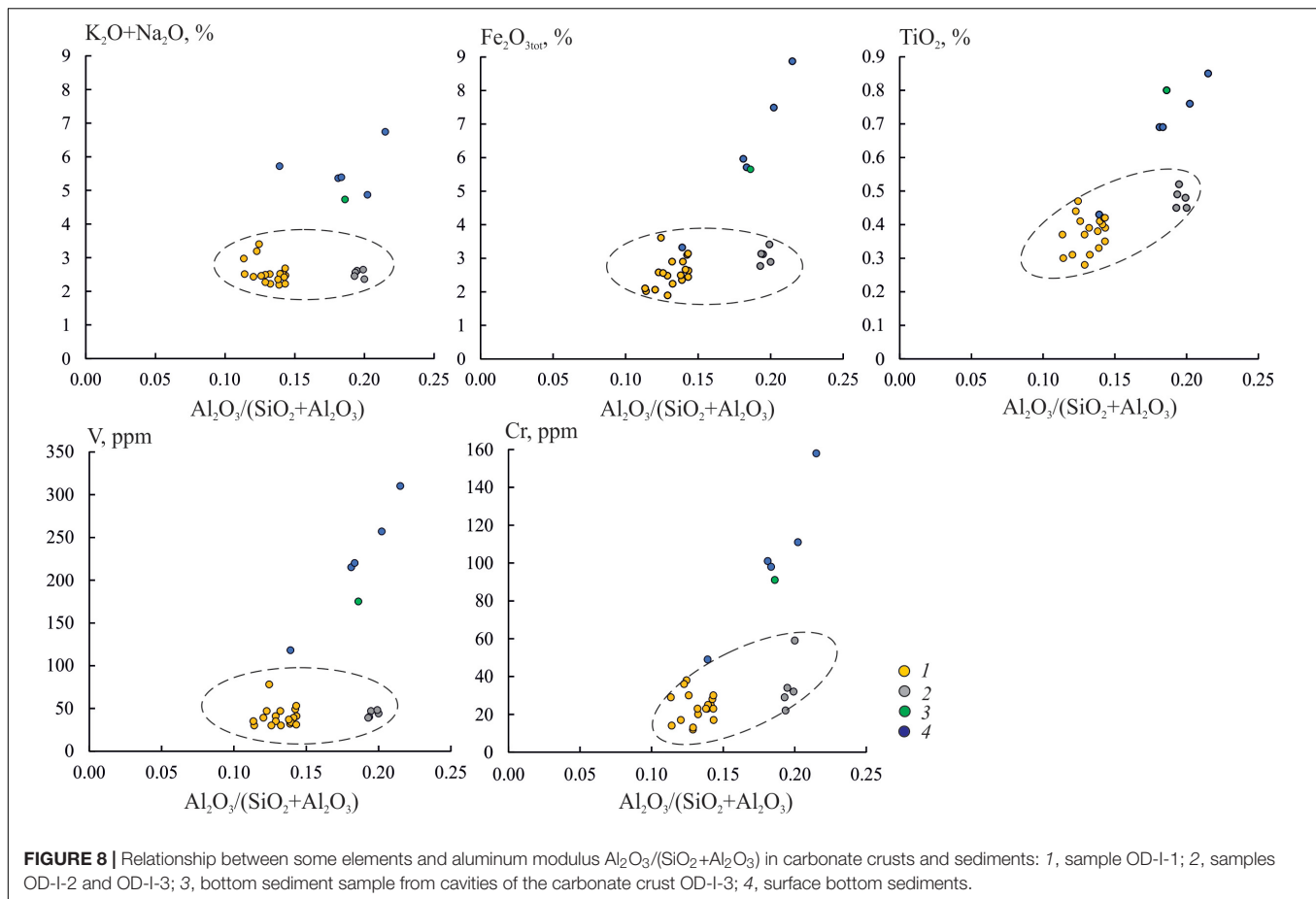


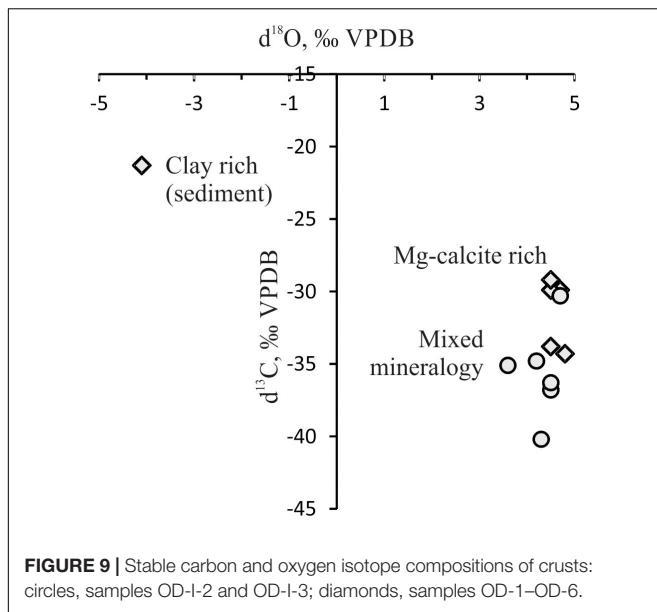
Table 1 give a higher temperature which can reach of 70–80°C, while the observed near-bottom temperature is only -1.77°C . Of course, carbon isotope disequilibrium between dissolved CO_2 and CH_4 in modern sediments can be explained by the kinetic fractionation during the AOM. However, we cannot exclude the involvement of isotopically heavy carbon of thermogenic methane from underlying hydrocarbon reservoir. To estimate the share of thermogenic methane included in the total dissolved methane of sediments we used the material balance eq. (4):

$$\delta^{13}\text{C}_{\text{TD}} = x(\delta^{13}\text{C}_{\text{TG}}) + (1 - x)(\delta^{13}\text{C}_{\text{MB}}), \quad (4)$$

where TD, TG, and MB is total dissolved, thermogenic, and microbial methane, respectively, and x is the part of thermogenic methane. We assume that $\delta^{13}\text{C}$ values of mixed methane sources are $-75 \pm 5\text{‰}$ VPDB (average value from **Table 1**), $-40 \pm 10\text{‰}$ VPDB – general value for thermogenic methane (Milkov and Etiope, 2018), and $-110 \pm 10\text{‰}$ VPDB – methane in equilibrium with carbonate of crusts. Using the equation (4) we estimate that the input of thermogenic gas into the total pull of dissolved methane of modern sediments can be significant and range from 30 to 70%.

To our knowledge, the $\delta^{13}\text{C}$ values of methane are usually 25–30‰ VPDB lower than the $\delta^{13}\text{C}$ values of an authigenic carbonate (Lein et al., 1999). Consequently, if one assumes

that all inorganic carbon in the carbonates is derived from degraded microbial methane, which is usually never the case, the $\delta^{13}\text{C}$ of CH_4 which generated the carbonate of studied carbonates should range from -55 to -70‰ VPDB. However, the $\delta^{13}\text{C}$ values of dissolved methane from the studied sediments are generally lower (from -71 to -78‰ VPDB, **Table 1**) and much lower calculated values of fossil methane equilibrated with carbonates (from -98 to -117‰ VPDB). In any case the estimated isotopic composition of the methane does not reflect the composition of the dissolved methane of “host” sediments. We do not exclude that methane, which is involved in carbonate precipitation, should involve some portion of the ^{13}C -enriched carbon. The $\delta^{13}\text{C}$ values of thermogenic methane from near-surface sediments of the Laptev Sea ranged from -37.4 to -42.8‰ VPDB (Cramer and Franke, 2005). If we assume that the participation of thermogenic methane in carbonate crust generation takes place, one may observe that the contribution of thermogenic methane should be considerable. According to the material balance equation, the addition of 58%–77% of thermogenic methane with a $\delta^{13}\text{C}$ value of approximately -40‰ VPDB to microbial methane needed to generate the carbonate crusts with the observed $\delta^{13}\text{C}$ - CaCO_3 values. Moreover, if we assume that microbial methane inherits the carbon isotope composition of the *in situ* OM ($-27.6 \pm 2\text{‰}$, **Table 6**), we can



estimate that the thermogenic methane contribution can be between 10% and 40%.

The review paper by Abrams (2017) has clearly demonstrated that microbial processes in sediments may mask the primary geochemical signature of migrating gas. It should be noted that integrating the geochemical data of near-surface sediments and geological setting (including tectonics, source rocks and related maturities) is needed to provide reliable interpretations. Therefore, carbon isotopic values of studied carbonates are ^{13}C -depleted ($\delta^{13}\text{C}\text{-CaCO}_3$ varied approximately from -30‰ to -40‰ VPDB) and with $\delta^{18}\text{O}$ up to 4.8‰ VPDB (Tables 5, 6), indicating a methanogenic origin, possibly linked to gas hydrate dissociation and offshore hydrocarbon reservoir partially overlapped by GHSZ and subsea permafrost. It should be noted that all of these methane sources have not been sufficiently studied yet in the Laptev Sea.

Oxygen isotopes (Table 5) of carbonates indicated that the temperature or fluid did not change significantly (Bohrmann et al., 1998; Lein, 2004; Mazzini et al., 2016) and was close to modern seawater at the observed temperatures of -1.77°C . The absence of significant variation in the $\delta^{18}\text{O}$ values of carbonates indicates the absence of significant fluctuations in the bottom water temperature during carbonate precipitation (Figure 9). Marine conditions similar to those of the modern era were established approximately 10.5–8.5 ka in the Laptev Sea (Spielhagen et al., 2005; Klyuyvitkina et al., 2009). That is, in the process of the polar front shifting to the north in the Atlantic Ocean and the penetration of warm Atlantic waters into the sea. Analogous to other Arctic seeps, methane seepage was controlled by the last deglaciation, which triggered changes in the fault system and favored gas migration. Currently, the flow of bubble-jet methane does not seem to induce the formation of authigenic carbonate pavements on the seafloor of the East-Siberian Shelf.

Consequently, predominantly microbial methane source with possibly thermogenic contribution of around 10.5–8.5 ka could have participated in precipitation of the studied MDAC below

the sediment-water interface. However, we found no isotopic evidence to support our hypothesis, other than data from Cramer and Franke (2005). But previous studies from other Arctic gas hydrate systems also found indications for elevated methane seepage related to the retreat of the glacial ice shield during an interglacial epoch (Andreassen et al., 2017; Schneider et al., 2018; Himmler et al., 2019; Yao et al., 2020). The occurrence of carbonate crusts on the seafloor in the area of active methane seepage is an indicator of exhumation following carbonate precipitation in the shallow subsurface of the Laptev Sea shelf. This phenomenon is widespread in continental margin environments and elsewhere (Naehr et al., 2007).

CONCLUSION AND PERSPECTIVE

Newly discovered crusts of methane-derived authigenic carbonate deposits were observed on the seafloor and sampled at *Oden* cold seep field with an area of approximately 13 km^2 on the outer shelf of the Laptev Sea. These MDACs are located inside the cold seep field, indicating that widespread carbonate precipitation is restricted to these locations. Seafloor observations indicated evidence of gas flares, and microbial colonies were recorded in the southern *Oden* area, suggesting that the seep field is currently active. This suggests that the seep field is currently an active fluid flow conduit.

The crusts containing fingerprints of gas mixtures could be the result of the physical mixing of different methane pools in response to the vertical and lateral diffusion of gas. This mixing involves admixtures of thermogenic and microbial gasses as well as an admixture of bicarbonate from seawater. Therefore, both thermogenic methane and microbial methane participated in the carbonate precipitation. The former plays a dominant role in MDAC formation. Methane oxidation coupled with pore water sulfate reduction was supported by abundant marcasite observed within the carbonate cements.

Methane cold seepage is related to deep-seated faults belonging to the Laptev Sea Rift System and the Khatanga-Lomonosov Fracture Zone. A similar origin of methane seepage has been reported in sediment deposits within Arctic seas at $72^\circ\text{--}79^\circ\text{ N}$. The source of methane may have originated from microbial oxidation of methane ongoing at the moment of carbonate precipitation and possibly linked to gas reservoir beneath the caprock formed by permafrost and GHSZ. We consider that the methane seepage could have been controlled by the last deglaciation that triggered changes in the fault system and favored gas migration from destabilized intrapermafrost gas hydrates and offshore hydrocarbon reservoir.

Currently available data on carbonate formation in the Siberian Arctic seas have reported that the MDAC can form in recent sub-surface sediments but cannot form pavements or large carbonate slabs at the sediment/water interface. The studied crusts have been exposed to seawater for a significant period, as highlighted by the outer surface microdissolution and absence of crystal growth of other carbonate phases. The mineral and chemical compositions of clastic particles (including clay minerals) cemented in crusts, and the formation of the surface layer of “host” sediments have noticeable differences.

This suggests ancient carbonate precipitation below the seafloor surface. Then, crusts have been uplifted and winnowed in the past. Although active seepage sites are observed within the study area, the evidence collected indicates that the retrieved carbonates are the result of paleo-methane seepage.

In this study, we explored the origin of MDAC on the seafloor of the Laptev Sea. The present study provides insights and directions for further research on cold seep systems in the Laptev Sea. An important data gap in the Siberian Arctic seas should be addressed by a detailed study of the U-Th carbonate age to determine carbonate precipitation rates and to provide new insights on the intensity of past methane seepage in the Arctic.

DATA AVAILABILITY STATEMENT

The original contributions presented in the study are included in the article/**Supplementary Material**, further inquiries can be directed to the corresponding author.

AUTHOR CONTRIBUTIONS

MK, AL, and MF proposed conceptualization. AL suggested methodology. MK, BB, ED, and OD contributed to the design of the study. MK organized the database. MK, AM, ED, OD, AB, and AS carried out formal analysis. MF, AM, and BB carried out investigation. MK and AL wrote the first draft of the manuscript. BB, ED, and OD wrote the sections of the manuscript. MF administered the project. All authors contributed to manuscript revision, read, and approved the submitted version.

REFERENCES

- Abrams, M. A. (2017). Evaluation of near-surface gases in marine sediments to assess subsurface petroleum gas generation and entrapment. *Geosciences* 7:35. doi: 10.3390/geosciences7020035
- Aloisi, G., Bouloubassi, I., Heijs, S. K., Pancost, R. D., Pierre, C., Sinninghe Damsté, J. S., et al. (2002). CH₄-consuming microorganisms and the formation of carbonate crusts at cold seeps. *Earth Planet Sci. Lett.* 203, 195–203. doi: 10.1016/S0012-821X(02)00878-6
- Andreassen, K., Hubbard, A., Winsborrow, M., Patton, H., Vadakkepuliambatta, S., Plaza-Faverola, A., et al. (2017). Massive blow-out craters formed by hydrate-controlled methane expulsion from the Arctic seafloor. *Science* 356, 948–953. doi: 10.1126/science.aal4500
- Argentino, C., Waghorn, K. A., Vadakkepuliambatta, S., Polteau, S., Bünz, S., and Panieri, G. (2021). Dynamic and history of methane seepage in the SW Barents Sea: new insights from Leirdjupet Fault Complex. *Sci. Rep.* 11:4373. doi: 10.1038/s41598-021-83542-0
- Åström, E. K. L., Carroll, M. L., Ambrose, W. G. Jr., Sen, A., Silyakova, A., et al. (2018). Methane cold seeps as biological oases in the high-Arctic deep sea. *Limnol. Oceanogr.* 63, S209–S231. doi: 10.1002/lno.10732
- Åström, E. K. L., Sen, A., Carroll, M. L., and Carroll, J. (2020). Cold seeps in a warming arctic: insights for benthic ecology. *Front. Mar. Sci.* 7:244. doi: 10.3389/fmars.2020.00244
- Baranov, B., Galkin, S., Vedenin, A., Dozorova, K., Gebruk, A., and Flint, M. (2020). Methane seeps on the outer shelf of the Laptev Sea: characteristic features, structural control, and benthic fauna. *Geo-Marine Lett.* 40, 1–17. doi: 10.1007/s00367-020-00655-7
- Baranov, B. V., Flint, M. V., Rimsky-Korsakov, N. A., Poyarkov, S. G., and Dozorova, K. A. (2018). Structural evidence of recent activity of the Khatanga–Lomonosov Fault Zone in the Laptev Sea. *Doklady Earth Sci.* 480, 344–347. doi: 10.1134/S1028334X18050215
- Bates, N. R., Mathis, J. T., and Cooper, L. W. (2009). Ocean acidification and biologically induced seasonality of carbonate mineral saturation states in the western Arctic Ocean. *J. Geophys. Res. Oceans* 114:11. doi: 10.1029/2008JC004862
- Bayon, G., Henderson, G. M., and Bohn, M. (2009). U–Th stratigraphy of a cold seep carbonate crust. *Chem. Geol.* 260, 47–56. doi: 10.1016/j.chemgeo.2008.11.020
- Bayon, G., Pierre, C., Etoubleau, J., Voisset, M., Cauquil, E., Marsset, T., et al. (2007). Sr/Ca and Mg/Ca ratios in Niger Delta sediments: Implications for authigenic carbonate genesis in cold seep environments. *Mar. Geol.* 241, 93–109. doi: 10.1016/j.margeo.2007.03.007
- Bezrukov, P. L., and Lisitzin, A. P. (1960). Classification of bottom sediments in modern marine reservoirs. *Trudy Inst. Oceanol.* 32, 3–14.
- Bian, Y., Feng, D., Roberts, H. H., and Chen, D. (2013). Tracing the evolution of seep fluids from authigenic carbonates: Green Canyon, northern Gulf of Mexico. *Mar. Petroleum Geol.* 44, 71–81. doi: 10.1016/j.marpetgeo.2013.03.010
- Bischoff, W. D., Bishop, F. C., and Mackenzie, F. T. (1983). Biogenically produced magnesian calcite; in homogeneities in chemical and physical properties; comparison with synthetic phases. *Am. Mineral.* 68, 1183–1188.
- Boetius, A., Ravensschlag, K., Schubert, C. J., Rickert, D., Widdel, F., Gleseke, A., et al. (2000). A marine microbial consortium apparently mediating anaerobic oxidation methane. *Nature* 407, 623–626. doi: 10.1038/35036572
- Bogoyavlensky, V., Kazanin, G., and Kishankov, A. (2018). Dangerous gas saturated objects in the world ocean: the Laptev Sea. *Drill. Oil* 5, 20–29.
- Bohrmann, G., Greinert, J., Suess, E., and Torres, M. (1998). Authigenic carbonates from the Cascadia subduction zone and their relation to gas hydrate stability. *Geology* 26, 647–650.

FUNDING

This study and article preparation was supported by the Russian Science Foundation through grant no. 20-17-00157. AM was supported by the Russian Foundation for Basic Research through grant no. 18-05-60246. ED was supported by the Russian Science Foundation through grant no. 18-17-00089. AS was supported by the Russian Foundation for Basic Research through grant no. 20-04-00487. Field studies were supported by the state budget through financing of marine expeditions. This article was carried out within the framework of state assignment, subject No. 0128-2021-0006.

ACKNOWLEDGMENTS

We acknowledge the participants of the 69rd cruise of the RV *Akademik Mstislav Keldysh* carried out in September 2017 for helping acquire the samples and seafloor images of MDAC. We would like to thank Andrey Vedenin and Sergey Galkin (IO RAS) for assisting with collecting the MDAC, and Anton Yakushev (IGEM RAS) and Tatiana Prusakova (FRC Biotechnology) for their assistance in analyses proceeding. We would also like to thank Editage (www.editage.com) for English language editing.

SUPPLEMENTARY MATERIAL

The Supplementary Material for this article can be found online at: <https://www.frontiersin.org/articles/10.3389/fmars.2021.690304/full#supplementary-material>

- Bottinga, Y. (1969). Calculated fractionation factors for carbon and hydrogen isotope exchange in the system calcite-carbon dioxide-graphite-methane-hydrogen-water vapor. *Geochim. Cosmochim. Acta* 33, 49–64. doi: 10.1016/0016-7037(69)90092-1
- Brücher, V., Bröder, L., Sawicka, J. E., Tesi, T., Joye, S. P., Sun, X., et al. (2018). Carbon mineralization in Laptev and East Siberian sea shelf and slope sediment. *Biogeosciences* 15, 471–490. doi: 10.5194/bg-15-471-2018
- Chacko, T., and Deines, P. (2008). Theoretical calculation of oxygen isotope fractionation factors in carbonate systems. *Geochim. Cosmochim. Acta* 72, 3642–3660. doi: 10.1016/j.gca.2008.06.001
- Chuvilin, E., Davletshina, D., Ekimova, V., Bukhanov, B., Shakhova, N., and Semiletov, I. (2019). Role of warming in destabilization of intrapermafrost gas hydrates in the arctic shelf: experimental modeling. *Geosciences* 9:407. doi: 10.3390/geosciences9100407
- Cramer, B., and Franke, D. (2005). Indications for an active petroleum system in the Laptev Sea, NE Siberia. *J. Petrol. Geol.* 28, 369–384. doi: 10.1111/j.1747-5457.2005.tb00088.x
- Crémière, A., Lepland, A., Chand, S., Sahy, D., Condon, D. J., Noble, S. R., et al. (2016a). Timescales of methane seepage on the Norwegian margin following collapse of the Scandinavian Ice Sheet. *Nat. Commun.* 7:11509. doi: 10.1038/ncomms11509
- Crémière, A., Lepland, A., Chand, S., Sahy, D., Kirsimäe, K., Bau, M., et al. (2016b). Fluid source and methane-related diagenetic processes recorded in cold seep carbonates from the Alveim channel, central North Sea. *Chem. Geol.* 432, 16–33. doi: 10.1016/j.chemgeo.2016.03.019
- Dean, J. F., Middelburg, J. J., Rökmann, T., Aerts, R., Blauw, L. G., Egger, M., et al. (2018). Methane feedbacks to the global climate system in a warmer world. *J. Am. Geophys. Union* 56, 207–250. doi: 10.1002/2017RG000559
- Demina, L. L., and Galkin, S. V. (2018). Ecology of the bottom fauna and bioaccumulation of trace metals along the Lena River–Laptev Sea transect. *Environ. Earth Sci.* 77:43. doi: 10.1007/s12665-018-7231-y
- Devol, A. H., and Ahmed, S. I. (1981). Are high rates of sulphate reduction associated with anaerobic oxidation of methane? *Nature* 291, 407–408. doi: 10.1038/291407a0
- Drachev, S. S. (2000). Laptev Sea rifted continental margin: modern knowledge and unsolved questions. *Polarforschung* 68, 41–50.
- Egger, M., Riedinger, N., Mogollin, J. M., and Jørgensen, B. B. (2018). Global diffusive fluxes of methane in marine sediments. *Nat. Geosci.* 11, 421–425. doi: 10.1038/s41561-018-0122-8
- Fisher, R. E., Sriskantharajah, S., Lowry, D., Lanoisellé, M., Fowler, C. M. R., James, R. H., et al. (2011). Arctic methane sources: isotopic evidence for atmospheric inputs. *Geophys. Res. Lett.* 38:L21803. doi: 10.1029/2011GL049319
- Flint, M. V., Poyarkov, S. G., and Rymisky-Korsakov, N. A. (2016). Ecosystems of the Russian Arctic-2015 (63rd cruise of the research vessel Akademik Mstislav Keldysh). *Oceanology* 56, 459–461. doi: 10.1134/S0001437016030061
- Flint, M. V., Poyarkov, S. G., and Rymisky-Korsakov, N. A. (2018). Ecosystems of the Siberian Arctic Seas-2017 (cruise 69 of the R/V Akademik Mstislav Keldysh). *Oceanology* 58, 315–318. doi: 10.1134/S0001437018020042
- Franke, D., Hinz, K., and Oncken, O. (2001). The Laptev sea rift. *Mar. Petrol. Geol.* 18, 1083–1127. doi: 10.1016/S0264-8172(01)00041-1
- Galimov, E. M., Kodina, L. A., Stepanets, O. V., and Korobeinik, G. S. (2006). Biogeochemistry of the Russian Arctic. Kara Sea: research results under the SIRRO project, 1995–2003. *Geochem. Int.* 44, 1053–1104. doi: 10.1134/S0016702906110012
- Gramberg, I. S., Demenitskaya, R. M., and Sekretov, S. B. (1990). The system of rift grabens of the Laptev Sea shelf as a missing link in the rift belt of the Gakkell Ridge – Morsk Rift. *Doklady Earth Sci.* 311, 689–694.
- Grasshoff, K., Kremling, K., and Ehrhardt, M. (2007). *Methods of Seawater Analysis: Third, Completely Revised and Extended Edition*. Hoboken, NJ: Wiley Blackwell, 1–600.
- Gusev, E. A., Zayonchek, A. V., Mennies, M. V., Rekant, P. V., Roudoy, A. S., Rybakov, K. S., et al. (2002). *The end of the Gakkell Ridge in the Laptev Sea. Geological-Geophysical Features of the Lithosphere of the Arctic Region* 4. St. Petersburg: VNIIOkeangeologia, 40–54.
- Hedges, J. I., and Mann, D. C. (1979). The lignin geochemistry of marine sediments from the southern Washington coast. *Geochim. Cosmochim. Acta* 43, 1809–1818. doi: 10.1016/0016-7037(79)90029-
- Himmler, T., Sahy, D., Martma, T., Bohrmann, G., Plaza-Faverola, A., Bünz, S., et al. (2019). A 160,000-year-old history of tectonically controlled methane seepage in the Arctic. *Sci. Adv.* 5:eaaw1450. doi: 10.1126/sciadv.aaw1450
- Hong, W.-L., Torres, M. E., Carroll, J. L., Crémière, A., Panieri, G., Yao, H., et al. (2017). Seepage from an arctic shallow marine gas hydrate reservoir is insensitive to momentary ocean warming. *Nat. Commun.* 8:15745. doi: 10.1038/ncomms15745
- Horita, J. (2001). Carbon isotope exchange in the system CO₂-CH₄ at elevated temperatures. *Geochim. Cosmochim. Acta* 65, 1907–1919. doi: 10.1016/S0016-7037(01)00570-1
- Jakobsson, M., Mayer, L., Coakley, B., Dowdeswell, J. A., Forbes, S., Fridman, B., et al. (2012). The International Bathymetric Chart of the Arctic Ocean (IBCAO) Version 3.0. *Geophys. Res. Lett.* 39:L12609. doi: 10.1029/2012GL052219
- James, R. H., Bousquet, P., Bussmann, I., Haeckel, M., Kipfer, R., Leifer, I., et al. (2016). Effects of climate change on methane emissions from seafloor sediments in the Arctic Ocean: a review. *Limnol. Oceanogr.* 61, S283–S299. doi: 10.1002/lno.10307
- Joseph, C., Campbell, K. A., Torres, M. E., Martin, R. A., Pohlman, J. W., Riedel, M., et al. (2013). Methane-derived authigenic carbonates from modern and paleoseeps on the *Cascadia margin*: mechanisms of formation and diagenetic signals. *Paleogeogr. Paleoclimatol. Paleocool.* 390, 52–67. doi: 10.1016/j.palaeo.2013.01.012
- Judd, A., and Hovland, M. (2007). *Seabed Fluid Flow – The Impact on Geology, Biology and the Marine Environment*. Cambridge: Cambridge University Press.
- Klyuvitkina, T. S., Novichkova, Y. A., Polyakova, Y. I., and Matthiessen, J. (2009). “Aquatic palynomorphs in the Eurasian Arctic Sea sediments and their significance for the late Pleistocene and Holocene paleoceanographic reconstructions (by the example of the White and the Laptev seas),” in *System of the Laptev Sea and the Adjacent Arctic Seas: Modern and Past Environments*, eds H. Kassens, A. P. Lisitzin, J. Thiede, Y. I. Polyakova, L. A. Timokhov, and I. E. Frolov (Moscow: Moscow State University Publishing House), 448–466.
- Knittel, K., and Boetius, A. (2009). Anaerobic oxidation of methane: progress with an unknown process. *Annu. Rev. Microbiol.* 63, 311–334. doi: 10.1146/annurev.micro.61.080706.093130
- Kravchishina, M. D., Lein, A. Y., Savvichev, A. S., Reykhard, L. E., Dara, O. M., and Flint, M. V. (2017). Authigenic Mg-calcite at a cold methane seep site in the Laptev Sea. *Oceanology* 57, 174–191. doi: 10.1134/S0001437017010064
- Krylov, A. A., Logvina, E. A., Matveeva, T. V., Prasolov, E. M., Sapega, V. F., Demidova, A. L., et al. (2015). Ikaite (CaCO₃ · 6H₂O) in bottom sediments of the Laptev Sea and the role of anaerobic methane oxidation in this mineral-forming process. *Russian Mineral. Soc. Lett.* 144, 61–75.
- Kulm, L. D., Suess, E., Moore, J. C., Carson, B., Lewis, B. T., Ritger, S. D., et al. (1986). Oregon subduction zone: venting, Fauna, and carbonates. *Science* 231, 561–566. doi: 10.1126/science.231.4738.561
- Lapham, L., Marshall, K., Magen, C., Lyubchich, V., Cooper, L. W., and Grebmeier, J. M. (2017). Dissolved methane concentrations in the water column and surface sediments of Hanna Shoal and Barrow Canyon, Northern Chukchi Sea. *Deep Sea Res. Part II Top. Stud. Oceanogr.* 144, 92–103. doi: 10.1016/j.dsr2.2017.01.00
- Lein, A., Vogt, P., Crane, K., Egorov, A., and Ivanov, M. (1999). Chemical and isotopic evidence for the nature of the fluid in CH₄-containing sediments of the Håkon Mosby Mud Volcano. *Geo-Mar Lett.* 19, 76–83. doi: 10.1007/s003670050095
- Lein, A. Y. (1984). Anaerobic consumption of organic matter in modern marine sediments. *Nature* 312, 148–150. doi: 10.1038/312148a0
- Lein, A. Y. (2004). Authigenic carbonate formation in the ocean. *Lithol. Min. Resourc.* 39, 1–30. doi: 10.1023/B:LIMI.0000010767.52720.8f
- Lein, A. Y., Makkaveev, P. N., Savvichev, A. S., Kravchishina, M. D., Belyaev, N. A., Dara, O. M., et al. (2013). Transformation of suspended particulate matter into sediment in the Kara Sea in September of 2011. *Oceanology* 53, 570–606. doi: 10.1134/S0001437013050081
- Lein, A. Y., Rusanov, I. I., Savvichev, A. S., Pimenov, N. V., Miller, Y. M., Ivanov, M. V., et al. (1996). Biogeochemical processes of the sulfur and carbon cycles in the Kara Sea. *Geochem. Int.* 34, 925–941.
- Lein, A. Y., Savvichev, A. S., Rusanov, I. I., Pavlova, G. A., Belyaev, N. A., Craine, K., et al. (2007). Biogeochemical processes in the Chukchi Sea. *Lithol. Min. Resourc.* 42, 221–239. doi: 10.1134/S0024490207030029
- Levin, L. A., Baco, A. R., Bowden, D. A., Colaco, A., Cordes, E. E., Cunha, M. R., et al. (2016). Hydrothermal vents and methane seeps: rethinking the sphere of influence. *Front. Mar. Sci.* 3:72. doi: 10.3389/fmars.2016.00072
- Lisitzin, A. P. (1996). *Oceanic Sedimentation: Lithology and Geochemistry*. Washington, DC: American Geophysical Union.
- Logvina, E., Krylov, A., Taldenkova, A., Blinova, V., Sapega, V., Novikhin, A., et al. (2018). Mechanisms of Late Pleistocene authigenic Fe–Mn-carbonate

- formation at the Laptev Sea continental slope (Siberian Arctic). *Arktos* 4:2. doi: 10.1007/s41063-018-0036-0
- Lu, Y., Sun, X., Xu, H., Konishi, H., Lin, Z., Xu, L., et al. (2018). Formation of dolomite catalyzed by sulfate-driven anaerobic oxidation of methane: mineralogical and geochemical evidence from the northern South China Sea. *Am. Mineral.* 103, 720–734. doi: 10.2138/am-2018-6226
- Macdonald, R. W., Kuzky, Z. Z. A., and Johannessen, S. C. (2015). The vulnerability of arctic shelf sediments to climate change. *Environ. Rev. Natl. Res. Council Canada* 23, 461–479. doi: 10.1139/er-2015-0040
- Marlow, J. J., Steele, J. A., Ziebis, W., Thurber, A. R., Levin, L. A., and Orphan, V. J. (2014). Carbonate-hosted methanotrophy represents an unrecognized methane sink in the deep sea. *Nat. Commun.* 5:5094. doi: 10.1038/ncomms6094
- Mau, S., Römer, M., Torres, M. E., Bussmann, I., Pape, T., Damm, E., et al. (2017). Widespread methane seepage along the continental margin off Svalbard – from Bjørnøya to Kongsfjorden. *Sci. Rep.* 7:42997. doi: 10.1038/srep42997
- Mazzini, A., Svensen, H. H., Planke, S., Forsberg, C. F., and Tjelta, T. I. (2016). Pockmarks and methanogenic carbonates above the giant Troll gas field in the Norwegian North Sea. *Mar. Geol.* 373, 26–38. doi: 10.1016/j.margeo.2015.12.012
- McAuliffe, C. (1971). Gas chromatographic determination of solutes by multiple phase equilibrium. *Chem. Technol.* 1, 46–51.
- Milkov, A. V., and Etiope, G. (2018). Revised genetic diagrams for natural gases based on a global dataset of >20,000 samples. *Organ. Geochem.* 125, 109–120. doi: 10.1016/j.orggeochem.2018.09.002
- Milkov, A. V., Sassen, R., Apanasovich, T. V., and Dadashev, F. G. (2003). Global gas flux from mud volcanoes: a significant source of fossil methane in the atmosphere and the ocean. *Geophys. Res. Lett.* 30:1037. doi: 10.1029/2002GL016358
- Naehr, T. H., Eichhubl, P., Orphan, V. J., Hovland, M., Paull, C. K., Ussler, W., et al. (2007). Authigenic carbonate formation at hydrocarbon seeps in continental margin sediments: a comparative study. *Deep Sea Res. Part II Top. Stud. Oceanogr.* 54, 1268–1291. doi: 10.1016/j.dsr2.2007.04.010
- Niemistö, L. (1974). A gravity corer for studies of soft sediments. *Merentutkimuslaitoksen Julkaisuja/Havsforskn-ingsinstitutets Skrifter* 238, 33–38.
- Nürnberg, D., Fütterer, D. K., Niessen, F., Nørgaard-Pedersen, N., Schubert, C. J., Spielhagen, R. F., et al. (1995). The depositional environment of the Laptev Sea continental margin: preliminary results from the R/V Polarstern ARK IX-4 cruise. *Polar Res.* 14, 43–54. doi: 10.3402/polar.v14i1.6650
- O'Connor, F. M., Boucher, O., Gedney, N., Jones, C. D., Folberth, G. A., Coppel, R., et al. (2010). Possible role of wetlands, permafrost, and methane hydrates in the methane cycle under future climate change: a review. *Rev. Geophys.* 48:RG4005. doi: 10.1029/2010RG000326
- Oppo, D., De Siena, L., and Kemp, D. B. (2020). A record of seafloor methane seepage across the last 150 million years. *Sci. Rep.* 10:2562. doi: 10.1038/s41598-020-59431-3
- O'Reilly, S. S., Hryniewicz, K., Little, C. T. S., Monteys, X., Szczyk, M. T., Murphy, B. T., et al. (2014). Shallow water methane-derived authigenic carbonate mounds at the Codling Fault Zone, western Irish Sea. *Mar. Geol.* 357, 139–150. doi: 10.1016/j.margeo.2014.08.007
- Pankratova, N., Skorohod, A., Belikov, I., Elansky, N., Rakitin, V., Shtabkin, et al. (2018). Evidence of atmospheric response to methane emissions from the East Siberian Arctic shelf. *Geogr. Environ. Sustainab.* 11, 85–92. doi: 10.24057/2071-9388-2018-11-1-85-92
- Paull, C. K., Hecker, B., Commeau, R., Freeman-Lynde, R. P., Neumann, C., Corso, W. P., et al. (1984). Biological communities at the Florida Escarpment Resemble hydrothermal vent taxa. *Science* 226, 965–967. doi: 10.1126/science.226.4677.965
- Pauly, H. (1963). "Ikait", a new mineral from Greenland Arctic. *Arctic* 16, 263–264. doi: 10.14430/arctic3545
- Peckmann, J., Birgel, D., and Kiel, S. (2009). Molecular fossils reveal fluid composition and flow intensity at a Cretaceous seep. *Geology* 37, 847–850. doi: 10.1130/G25658A.1
- Peckmann, J., Reimer, A., Luth, U., Luth, C., Hansen, B. T., Heinicke, C., et al. (2001). Methane-derived carbonates and authigenic pyrite from the northwestern Black Sea. *Mar. Geol.* 177, 129–150. doi: 10.1016/S0025-3227(01)00128-1
- Peckmann, J., and Thiel, V. (2004). Carbon cycling at ancient methane-seeps. *Chem. Geol.* 205, 443–467. doi: 10.1016/j.chemgeo.2003.12.025
- Piskarev, A. L. (2016). *Arctic Basin (Geology and Morphology)*. St. Petersburg: VNIIOkeangeologia.
- Piskunova, E. A., Palshin, N. A., and Yakovlev, D. V. (2018). Electrical conductivity features of the Arctic shelf permafrost and electromagnetic technologies for their studies. *Russ. J. Earth. Sci.* 18:ES5001. doi: 10.2205/2018ES000628
- Plaza-Faverola, A., and Keiding, M. (2019). Correlation between tectonic stress regimes and methane seepage on the western Svalbard margin. *Solid Earth* 10, 79–94. doi: 10.5194/se-10-79-2019
- Prouty, N. G., Sahy, D., Ruppel, C. D., Roark, E. B., Condon, D., Brooke, S., et al. (2016). Insights into methane dynamics from analysis of authigenic carbonates and chemosynthetic mussels at newly-discovered Atlantic Margin seeps. *Earth Planet. Sci. Lett.* 449, 332–344. doi: 10.1016/j.epsl.2016.05.023
- Puglini, M., Brovkin, V., Brovkin, V., Regnier, P., and Arndt, S. (2020). Assessing the potential for non-turbulent methane escape from the East Siberian Arctic Shelf. *Biogeosciences* 17, 3247–3275. doi: 10.5194/bg-17-3247-2020
- Reeburgh, W. S. (2007). Oceanic methane biogeochemistry. *Chem. Rev.* 107, 486–513. doi: 10.1021/cr050362v
- Rekant, P., Bauch, H. A., Schwenk, T., Portnov, A., Gusev, E., Spiess, V., et al. (2015). Evolution of subsea permafrost landscapes in Arctic Siberia since the Late Pleistocene: a synoptic insight from acoustic data of the Laptev Sea. *Arktos* 1, 1–16. doi: 10.1007/s41063-015-0011-y
- Rekant, P. V., and Gusev, E. A. (2009). Signs of the newest tectonic movements of the Laptev Sea continental margin according to seismic profiling data. *Arctic Antarct. Res.* 2, 85–94.
- Roberts, H. H., and Feng, D. (2013). "3. Carbonate precipitation at Gulf of Mexico hydrocarbon seeps: an overview," in *Hydrocarbon Seepage*, eds D. L. Connolly, T. B. Berge, and F. Aminzadeh (Tulsa, OH: Society of Exploration Geophysicists and American Association of Petroleum Geologists), 43–61. doi: 10.1190/1.9781560803119.ch3
- Romanovskii, N. N., Eliseeva, A. A., Gavrilov, A. V., Tipenko, G. S., and Hubberten, H.-W. (2006). The long-term dynamics of the permafrost and gas hydrate stability zone on rifts of the East Siberian Arctic shelf (Report 2). *Earth's Cryosphere* 10, 29–38.
- Romanovskii, N. N., and Hubberten, H.-W. (2006). Permafrost and gas hydrate stability zone on the Laptev Sea shelf (main results of ten-year Russian-German investigation). *Earth's Cryosphere* 10, 61–68.
- Romanovskii, N. N., Hubberten, H.-W., Gavrilov, A. V., Eliseeva, A. A., and Tipenko, G. S. (2005). Offshore permafrost and gas hydrate stability zone on the shelf of East Siberian Seas. *Geo-Mar. Lett.* 25, 167–182. doi: 10.1007/s00367-004-0198-6
- Rothwell, R. G. (ed) (1989). "The smear slide method," in *Minerals and Mineraloids in Marine Sediments*, (Dordrecht: Springer).
- Ruban, A., Rudmin, M., Dudarev, O., and Mazurov, A. (2020). The formation of authigenic carbonates at a methane seep site in the northern part of the laptev sea. *Minerals* 10, 1–14. doi: 10.3390/min10110948
- Ruff, S. E., Biddle, J. F., Teske, A. P., Knittel, K., Boetius, A., and Ramette, A. (2015). Global dispersion and local diversification of the methane seep microbiome. *PNAS* 112, 4015–4020. doi: 10.1073/pnas.1421865112
- Sauer, S., Crémière, A., Knies, J., Lepland, A., Sahy, D., Martmad, T., et al. (2017). U-Th chronology and formation controls of methane-derived authigenic carbonates from the Hola Trough seep area, northern Norway. *Chem. Geol.* 470, 164–179. doi: 10.1016/j.chemgeo.2017.09.004
- Savvichev, A. S., Kadnikov, V. V., Kravchishina, M. D., Galkin, S. V., Novigatskii, A. N., Sigalevich, P. A., et al. (2018a). Methane as an organic matter source and the trophic basis of a Laptev Sea cold seep microbial community. *Geomicrobiol. J.* 35, 411–423. doi: 10.1080/01490451.2017.1382612
- Savvichev, A. S., Rusanov, I. I., Kadnikov, V. V., Beletskii, A. V., Ravin, N. V., and Pimenov, N. V. (2018b). Microbial community composition and rates of the methane cycle microbial processes in the upper sediments of the yamal sector of the Southwestern Kara Sea. *Microbiology* 87, 238–248. doi: 10.1134/S0026261718020121
- Savvichev, A. S., Zakharaeva, E. E., Veslopolova, E. F., Rusanov, I. I., Levin, A. Y., and Ivanov, M. V. (2010). Microbial processes of the carbon and sulfur cycles in the Kara Sea. *Oceanology* 50, 893–908. doi: 10.1134/S0001437010060093
- Schneider, A., Panieri, G., Lepland, A., Consolaro, C., Cr_emi_ere, A., Forwick, M., et al. (2018). Methane seepage at Vestnesa Ridge (NW svalbard) since the last

- glacial maximum. *Quat. Sci. Rev.* 193, 98–117. doi: 10.1016/j.quascirev.2018.06.006
- Schrag, D. P., Higgins, J. A., Macdonald, F. A., and Johnston, D. T. (2013). Authigenic carbonate and the history of the global carbon cycle. *Science* 339, 540–543. doi: 10.1126/science.1229578
- Schubert, C. J., Nürnberg, D., Scheele, N., Pauer, F., and Kriewis, M. (1997). ^{13}C isotope depletion in ikaite crystals: evidence for methane release from the Siberian shelves? *Geo-Mar. Lett.* 17, 169–174. doi: 10.1007/s003670050023
- Semiletov, I., Pipko, I., Gustafsson, Ö, Anderson, L. G., Sergienko, V., Pugach, S., et al. (2016). Acidification of East Siberian Arctic Shelf waters through addition of freshwater and terrestrial carbon. *Nat. Geosci.* 9, 361–365. doi: 10.1038/ngeo2695
- Semiletov, I. P., Shakhova, N. E., Pipko, I. I., Pugach, S. P., Charkin, A. N., Dudarev, O. V., et al. (2013). Space-time dynamics of carbon and environmental parameters related to carbon dioxide emissions in the Buor-Khaya Bay and adjacent part of the Laptev Sea. *Biogeosciences* 10, 5977–5996. doi: 10.5194/bg-10-5977-2013
- Semiletov, I. P., Shakhova, N. E., Sergienko, V. I., Pipko, I. I., and Dudarev, O. V. (2012). On carbon transport and fate in the East Siberian Arctic land-shelf-atmosphere System. *Environ. Res. Lett.* 7:015201. doi: 10.1088/1748-9326/7/1/015201
- Serov, P., Vadakkepuliambatta, S., Mienerta, J., Pattona, H., Portnova, A., Silyakova, A., et al. (2017). Postglacial response of Arctic Ocean gas hydrates to climatic amelioration. *PNAS* 114, 6215–6220. doi: 10.1073/pnas.1619288114
- Shakhova, N., Semiletov, I., Leifer, I., Sergienko, V., Salyuk, A., Kosmach, D., et al. (2014). Ebullition and storm-induced methane release from the East Siberian Arctic Shelf. *Nat. Geosci.* 7, 64–70. doi: 10.1038/ngeo2007
- Shakhova, N., Semiletov, I., Salyuk, A., Yusupov, V., Kosmach, D., and Gustafsson, Ö (2010). Extensive methane venting to the atmosphere from the sediments of the East Siberian Arctic shelf. *Science* 327, 1246–1250. doi: 10.1126/science.1182221
- Shakhova, N., Semiletov, I., Sergienko, V., Lobkovsky, L., Yusupov, V., Salyuk, A., et al. (2015). The East Siberian Arctic Shelf: towards further assessment of permafrost-related methane fluxes and role of sea ice. *Philos. Trans. R. Soc. A* 373:20140451. doi: 10.1098/rsta.2014.0451
- Shipilov, E. V. (2004). Tectono-geodynamic evolution of Arctic continental margins during epochs of young ocean formation. *Geotectonics* 38, 343–365.
- Shkarubo, S. I., Zavarzina, G. A., and Zuykova, O. N. (2014). Results of modern stage of the Laptev Sea shelf study: from hypotheses to new facts and problems. *Prospect Protect. Min. Resourc.* 4, 23–30.
- Skorokhod, A. I., Pankratova, N. V., Belikov, I. B., Thompson, R. L., Novigatsky, A. N., and Golitsyn, G. S. (2016). Observations of atmospheric methane and its stable isotope ratio ($\delta^{13}\text{C}$) over the Russian Arctic seas from ship cruises in the summer and autumn of 2015. *Doklady Earth Sci.* 470, 1081–1085. doi: 10.1134/S1028334X16100160
- Smrzka, D., Zwicker, J., Misch, D., Walkner, C., Gier, S., Monien, P., et al. (2019). Oil seepage and carbonate formation: a case study from the southern Gulf of Mexico. *Sedimentology* 66, 2318–2353. doi: 10.1111/sed.12593
- Smrzka, D. J., Zwicker, Y., Lu, Sun, Y., Feng, D., Monien, P., et al. (2021). Trace element distribution in methane-seep carbonates: the role of mineralogy and dissolved sulfide. *Chem. Geol.* 580:120357. doi: 10.1016/j.chemgeo.2021.120357
- Spielhagen, R. F., Erlenkeuser, H., Siebert, and Ch. (2005). History of freshwater runoff across the Laptev Sea (Arctic) during the last deglaciation. *Glob. Planet. Change* 48, 187–207. doi: 10.1016/j.gloplacha.2004.12.013
- Suess, E. (2014). Marine cold seeps and their manifestations: geological control, biogeochemical criteria and environmental conditions. *Int. J. Earth Sci.* 103, 1889–1916. doi: 10.1007/s00531-014-1010-0
- Tesi, T., Semiletov, I., Hugelius, G., Dudarev, O., Kuhry, P., and Gustafsson, Ö (2014). Composition and fate of terrigenous organic matter along the Arctic land-ocean continuum in East Siberia: insights from biomarkers and carbon isotopes. *Geochim. Cosmochim. Acta* 133, 235–256. doi: 10.1016/j.gca.2014.02.045
- Thornton, B. F., Geibel, M. C., Crill, P. M., Humborg, C., and Mörtz, C.-M. (2016). Methane fluxes from the sea to the atmosphere across the Siberian shelf seas. *Geophys. Res. Lett.* 43, 5869–5877. doi: 10.1002/2016GL068977
- Valentine, D. L. (2002). Biogeochemistry and microbial ecology of methane oxidation in anoxic environments: a review. *Antonie van Leeuwenhoek Int. J. Gen. Mol. Microbiol.* 81, 271–282. doi: 10.1023/A:1020587206351
- Valentine, D. L., and Reeburgh, W. S. (2000). New perspectives on anaerobic methane oxidation. *Environ. Microbiol.* 2, 477–484. doi: 10.1046/j.1462-2920.2000.00135.x
- Vedenin, A. A., Kokarev, V. N., Chikina, M. V., Basin, A. B., Galkin, S. V., and Gebruk, A. V. (2020). Fauna associated with shallow-water methane seeps in the Laptev Sea. *PeerJ* 8:e9018. doi: 10.7717/peerj.9018
- Weber, T., Wiseman, N. A., and Kock, A. (2019). Global ocean methane emissions dominated by shallow coastal waters. *Nat. Commun.* 10:4584. doi: 10.1038/s41467-019-12541-7
- Whitcar, M. J. (1999). Carbon and hydrogen isotope systematics of bacterial formation and oxidation of methane. *Chem. Geol.* 161, 291–314. doi: 10.1016/S0009-2541(99)00092-3
- Yamamoto-Kawai, M., McLaughlin, F. A., Carmack, E. C., Nishino, S., and Shimada, K. (2009). Aragonite undersaturation in the Arctic Ocean: effects of ocean acidification and sea ice melt. *Science* 326, 1098–1100. doi: 10.1126/science.1174190
- Yamamoto-Kawai, M., Mifune, T., Kikuchi, T., and Nishino, S. (2016). Seasonal variation of CaCO_3 saturation state in bottom water of a biological hotspot in the Chukchi Sea, Arctic Ocean. *Biogeosciences* 13, 6155–6169. doi: 10.5194/bg-13-6155-2016
- Yao, H., Niemann, H., and Panieri, G. (2020). Multi-proxy approach to unravel methane emission history of an Arctic cold seep. *Q. Sci. Rev.* 244:106490. doi: 10.1016/j.quascirev.2020.106490
- Yao, H., Panieri, G., Lehmann, M. F., Himmler, T., and Niemann, H. (2021). Biomarker and isotopic composition of seep carbonates record environmental conditions in two arctic methane seeps. *Front. Earth Sci.* 8:570742. doi: 10.3389/feart.2020.570742
- Yu, Z., Wang, X., Han, G., Liu, X., and Zhang, E. (2018). Organic and inorganic carbon and their stable isotopes in surface sediments of the Yellow River Estuary. *Sci. Rep.* 8:10825. doi: 10.1038/s41598-018-29200-4
- Yusupov, V. I., Salyuk, A. N., Karnaukh, V. N., Semiletov, I. P., and Shakhova, N. E. (2010). Detection of methane ebullition in shelf waters of the Laptev Sea in the Eastern Arctic Region. *Doklady Earth Sci.* 430, 261–264. doi: 10.1134/S1028334X1002025X
- Yvon-Durocher, G., Allen, A. P., Bastviken, D., Conrad, R., Gudas, C., St-Pierre, A., et al. (2014). Methane fluxes show consistent temperature dependence across microbial to ecosystem scales. *Nature* 507, 488–491. doi: 10.1038/nature13164
- Zhang, F., Xu, H., Konishi, H., Kemp, J. M., Roden, E. E., and Shen, Z. (2012). Dissolved sulfide-catalyzed precipitation of disordered dolomite: implications for the formation mechanism of sedimentary dolomite. *Geochim. Cosmochim. Acta* 97, 148–165. doi: 10.1016/j.gca.2012.09.008
- Zhang, F., Xu, H., Konishi, H., and Roden, E. E. (2010). A relationship between d_{104} value and composition in the calcite-disordered dolomite solid-solution series. *Am. Mineral.* 95, 1650–1656. doi: 10.2138/am.2010.3414

Conflict of Interest: The authors declare that the research was conducted in the absence of any commercial or financial relationships that could be construed as a potential conflict of interest.

Publisher's Note: All claims expressed in this article are solely those of the authors and do not necessarily represent those of their affiliated organizations, or those of the publisher, the editors and the reviewers. Any product that may be evaluated in this article, or claim that may be made by its manufacturer, is not guaranteed or endorsed by the publisher.

Copyright © 2021 Kravchishina, Lein, Flint, Baranov, Miroshnikov, Dubinina, Dara, Boev and Savvichev. This is an open-access article distributed under the terms of the Creative Commons Attribution License (CC BY). The use, distribution or reproduction in other forums is permitted, provided the original author(s) and the copyright owner(s) are credited and that the original publication in this journal is cited, in accordance with accepted academic practice. No use, distribution or reproduction is permitted which does not comply with these terms.